Physics of Fluids

Instabilities in viscosity-stratified two-fluid channel flow over an anisotropic-inhomogeneous porous bottom

Cite as: Phys. Fluids **31**, 012103 (2019); https://doi.org/10.1063/1.5065780
Submitted: 11 October 2018 . Accepted: 05 December 2018 . Published Online: 03 January 2019

Geetanjali Chattopadhyay, Usha Ranganathan, and Severine Millet

Instabilities in viscosity-stratified two-fluid channel flow over an anisotropic-inhomogeneous porous bottom

Cite as: Phys. Fluids 31, 012103 (2019); doi: 10.1063/1.5065780
Submitted: 11 October 2018 • Accepted: 5 December 2018 •
Published Online: 3 January 2019

View Online Export Citation CrossMark

Geetanjali Chattopadhyay,[1] Usha Ranganathan,[1,a)] and Severine Millet[2]

AFFILIATIONS

[1] Department of Mathematics, Indian Institute of Technology Madras, Chennai 600036, Tamilnadu, India
[2] Laboratoire de Mécanique des Fluides et d'Acoustique, CNRS/Université de Lyon, Ecole Centrale de Lyon/ Université Lyon 1/INSA de Lyon, ECL, 36 Avenue Guy de Collongue, 69134 Ecully, France

[a)] **Electronic mail**: ushar@iitm.ac.in

ABSTRACT

A linear stability analysis of a pressure driven, incompressible, fully developed laminar Poiseuille flow of immiscible two-fluids of stratified viscosity and density in a horizontal channel bounded by a porous bottom supported by a rigid wall, with anisotropic and inhomogeneous permeability, and a rigid top is examined. The generalized Darcy model is used to describe the flow in the porous medium with the Beavers-Joseph condition at the liquid-porous interface. The formulation is within the framework of modified Orr-Sommerfeld analysis, and the resulting coupled eigenvalue problem is numerically solved using a spectral collocation method. A detailed parametric study has revealed the different active and coexisting unstable modes: porous mode (manifests as a minimum in the neutral boundary in the long wave regime), interface mode (triggered by viscosity-stratification across the liquid-liquid interface), fluid layer mode [existing in moderate or O(1) wave numbers], and shear mode at high Reynolds numbers. As a result, there is not only competition for dominance among the modes but also coalescence of the modes in some parameter regimes. In this study, the features of instability due to two-dimensional disturbances of porous and interface modes in isodense fluids are explored. The stability features are highly influenced by the directional and spatial variations in permeability for different depth ratios of the porous medium, permeability and ratio of thickness of the fluid layers, and viscosity-stratification. The two layer flow in a rigid channel which is stable to long waves when a highly viscous fluid occupies a thicker lower layer can become unstable at higher permeability (porous mode) to long waves in a channel with a homogeneous and isotropic/anisotropic porous bottom and a rigid top. The critical Reynolds number for the dominant unstable mode exhibits a nonmonotonic behaviour with respect to depth ratio. However, it increases with an increase in anisotropy parameter ξ indicating its stabilizing role. Switching of dominance of modes which arises due to variations in inhomogeneity of the porous medium is dependent on the permeability and the depth ratio. Inhomogeneity arising due to an increase in vertical variations in permeability renders short wave modes to become more unstable by enlarging the unstable region. This is in contrast to the anisotropic modulations causing stabilization by both increasing the critical Reynolds number and shrinking the unstable region. A decrease in viscosity-stratification of isodense fluids makes the configuration hosting a less viscous fluid in a thinner lower layer adjacent to a homogeneous, isotropic porous bottom to be more unstable than the one hosting a highly viscous fluid in a thicker lower layer. An increase in relative volumetric flow rate results in switching the dominant mode from the interface to fluid layer mode. It is evident from the results that it is possible to exercise more control on the stability characteristics of a two-fluid system overlying a porous medium in a confined channel by manipulating the various parameters governing the flow configurations. This feature can be effectively exploited in relevant applications by enhancing/suppressing instability where it is desirable/undesirable.

I. INTRODUCTION

Viscosity/density stratified flows are more representative of real flows encountered in the environment and industry. Flow stability investigations have revealed that stratification in viscosity significantly affects the flow, and in some cases there are unexpected switching of dominance of unstable modes and coalescence of unstable modes. Such fascinating and interesting display of flow features of this system has motivated several studies, in a variety of situations. These studies have focussed on the understanding of stability characteristics of the two-fluid system in confined complex geometries that are crucial in many industrial applications and natural phenomena (oil-water two-phase flows, coextrusion of polymer melts, and cryolite/aluminium melts in a conventional reduction cell[1,2]).

Yiantsios and Higgins[3] have investigated the stability of Poiseuille flow of viscosity and density stratified superposed immiscible fluids in a rigid channel and have shown that the flow may be unstable to an interfacial mode at small Reynolds numbers and to a shear mode of the Tollmien-Schlichting type, if the Reynolds number is sufficiently large. Their predictions agree qualitatively with the experimental results of Kao and Park.[4] Tilley *et al.*[5] have extended the analysis by Yiantsios and Higgins,[3] and the conclusions are consistent with the results observed by Kaffel and Riaz[6] on the growth rates, the wave speeds, and the amplitudes of the perturbations of both the shear and interface modes of instability.

Apart from the above investigations, where a viscosity-stratification is achieved by considering immiscible fluids in contact with each other in a flow configuration with a discontinuity in viscosity across a sharp interface (interface dominated flows), there are other ways which include (i) varying the temperature or concentration continuously in which case a diffusive interface of nonzero thickness occurs and (ii) using a non-Newtonian fluid.[7] A recent review article by Govindarajan and Sahu[8] and the references therein have discussed in detail the instabilities arising due to viscosity-stratification. They have remarked in this article that, although it is important to gain knowledge about the nonlinear stages of growth of unstable modes and about how transition from laminar to turbulence occurs in simple flow systems, there are a number of issues to be addressed and understood in viscosity stratified systems, even in the linear regime that would help in improving the performance of many industrial processes and in understanding typical flow features in nature and environment.

The available literature on such investigations is large but mentioning some studies might reveal the current state of the art in viscosity stratified systems.[9,10] These studies have been performed in confined geometries with rigid walls, but there are a number of applications in which the structure of the solid surface adjacent to the fluid has a significant influence on the threshold for instability and on the growth/decay of the unstable waves.[11–19] This necessitates the inclusion of bottom permeability and porosity of the substrate, when the substrate is porous. This has led to increased interest on the investigations on stability characteristics and dynamics of fluid flows in confined geometries bounded by porous walls.[20–25] These studies have been sparked by the relevance of wall permeability in numerous applications such as in geophysics,[11,26,27] in biomechanics,[28,29] in aeronautics,[14,30–32] and in industry.[33,34]

There are also several applications in which the velocity of a viscous fluid demonstrates a tangential velocity slip at the walls. In fact, an apparent breakdown of the no-slip condition for Newtonian fluids near the solid substrates has been observed in the experiments on small scale pressure gradient and shear driven flows.[35–39] Such flows have displayed slip lengths (the ratio of the surface velocity to the surface shear rate) as large as microns. In addition, large slip lengths of the order of 50 μm have been observed in the case of grooved substrates.[39–42] The experiments by Ruckenstein and Rajora,[43] Tretheway and Meinhart,[44] and Watanabe and Udagawa[45] reveal that no-slip boundary condition is not appropriate for a hydrophilic liquid flow over hydrophobic boundaries both at micro- and nanoscales. These suggest that flow over rough or textured surfaces at the microscale and/or hydrophobic substrates can be addressed by modelling such substrates as smooth surfaces with an effective slip at the surface.[46]

Motivated by the experimental observations on the existence of velocity slip at a substrate and the theoretical predictions on the role of velocity slip in the stability characteristics on flow systems in confined configurations,[35–46] Chattopadhyay and Usha[25] have examined the stability features of a two-phase plane Poiseuille flow in a hydrophobic channel by modelling the channel walls as smooth surfaces with velocity slip. Their study reveals the possibility for controlling instabilities in interface dominated rigid channel flows by designing the walls of the channel as hydrophobic/rough/porous surfaces which can be modelled as one with slip at the substrate.

The above model does not incorporate the transport of fluid within the substrate (for example, within the underlying porous medium, if the substrate is porous), and it accounts for the dynamics only through the slip boundary condition; that is, the effects of the presence of a porous layer are reduced to a boundary condition at the liquid-porous interface. As a result, the coupling between the surface flow above and the subsurface flow (flow in the porous medium) is neglected. This in turn suppresses the porous-layer induced mode which is triggered by the presence of the porous layer. Furthermore, the stability characteristics predicted by the experimental investigations on Poiseuille flow of a single layer of Newtonian fluid in a porous channel[20,21,47,48] reveal that destabilisation of channel flow with permeable walls is more significant than that in a confined channel with impermeable walls. This has motivated a number of investigations on single layer and two-layer Poiseuille flow in a porous channel with isotropic and homogeneous permeability.[20–22,24,32,47–65]

There are also flows occurring in nature such as in solidification of multi-component melts or passage of wind through urban areas or forest canopies where we observe flow of fluids in domains across a macroscopic interface between a porous layer and a pure fluid. Such flows are also observed in various technological scenarios (air filtration systems and fuel cells). Due to their applicability, dynamics and stability of flows over porous layers have received considerable attention (flows in bounded domains such as Poiseuille flows,[47,48,53,66] Couette flows,[24,67] and free surface flows over inclined porous surfaces[68–72]).

The fluid flow over a porous medium incorporating thermal convection has been studied extensively.[32,73–80] The above studies have performed a linear stability analysis for the onset of natural convection by using the Darcy law in the porous region and the Stokes/Navier-Stokes equation in the fluid region along with the Beavers-Joseph (B-J) condition at the liquid-porous interface.[58,61]

There are also investigations based on a two-domain approach where Darcy-Brinkman equations are the governing equations in the porous layer[81–83] along with continuity of both velocity and tangential stress at the liquid-porous interface. Hirata *et al.*[80] have reported that neutral stability boundaries obtained using the above one and two domain approaches are in good agreement with a window [1, 4] of Beavers-Joseph constant α_{BJ}, for all depth ratios.

In fact, the problem of fluid flow at the porous medium/clean fluid interface has been first analysed by Beavers and Joseph,[58] and they have considered the Darcy law to describe the flow in the porous bottom. Larson and Higdon[84,85] have studied the momentum transport in the neighbourhood of the interface region, and a comprehensive survey of the literature is available on this subject.[49,86]

Chen and Chen[32] have addressed the thermal convective instability of a fluid layer above a porous layer which is heated from below. Their linear stability analysis predicts a bimodal structure in the neutral boundaries. According to them, the depth ratio, $\hat{d}$, plays a significant role. As $\hat{d}$ increases, there is a switching of the dominance of unstable mode. The mode which exists due to the onset of instability occurring in both the porous and the fluid layers and characterized by its presence in the left hand lobe of the zero contour of the linear growth rate in the $\alpha - Re$ parameter regime is the porous layer mode.[87] The stability of this mode is controlled by the porous medium. If the onset of instability is within the layer of fluid and the unstable mode is characterized by its presence on the right side lobe of the neutral boundary, then the unstable mode is referred to as the odd fluid layer mode.[87] The fluid (porous) layer mode dominates for large (small) $\hat{d}$.

It is worth mentioning here that there is a wealth of results on the stability characteristics of flow of a single layer of fluid in a porous channel. This is apart from investigations on instabilities in such systems where instabilities due to the thermal convection[32,49,50] and dispersion-driven instability of mixed convective flow in porous media[88] are considered.

Chang *et al.*[48] have addressed the linear stability of a Poiseuille flow of a fluid overlying a porous medium saturated with the same fluid, for perturbations of arbitrary wave numbers within the framework of Orr-Sommerfeld analysis. The Darcy model along with the Beavers-Joseph interface condition at the porous-liquid interface has been employed to describe the dynamics in the porous medium. The resulting eigenvalue problem has been numerically solved using the Chebyshev tau method.[51,52] They have observed neutral boundaries with bi-modal and tri-modal structures as the depth ratio is varied. It is the shear stress which is responsible for triggering these instability modes. In addition to the two modes of instability shown by Chen and Chen,[32] they have observed a new unstable mode which manifests as a middle lobe on the neutral boundary. It is clear that the existence of this third mode of instability is due to fluid layer shear. This mode is referred to as the even fluid-layer mode in accordance with the even symmetry in the fluid layer displayed by the corresponding perturbation eigenfunction. Thus, even-fluid mode is associated with the local minimum of the middle lobe of the neutral boundary. The Beavers-Joseph condition at the liquid-porous (Darcy model) interface has been successfully employed in several investigations such as in the theoretical[89] and numerical[18,90,91] investigations, and these studies have justified the use of the Darcy model with the Beavers-Joseph condition. Furthermore, the existence of a weak solution proved by Layton *et al.*[92] for the flow through a Darcy porous medium with a fluid layer overlying it and governed by Stokes' equations with the Beavers-Joseph condition at the porous-liquid interface enhances one's confidence to employ the same in the formulation of stability problems involving a porous medium.

Subsequently, the Brinkman model with appropriate boundary conditions incorporating the viscous diffusion effects close to the porous-liquid interface has been employed,[47,53] and the stability features of pressure driven flow in a channel bounded by a porous bottom and a rigid wall at the top have been analysed. The experimental observations of Silin *et al.*[62] serve as validation of the above results.

Based on the suggestions by Nield,[74] a Brinkman model has been used in the boundary-layer region where the fluid enters the porous medium. Hill and Straughan[47] have revisited the problem and have examined the linear stability of Poiseuille flow problem in which a Newtonian fluid layer overlies a transition layer composed of a Brinkman model and this in turn overlies a Darcy porous layer. The fluid mode observed by Chang *et al.*[48] has been found to be absent in the result by Hill and Straughan,[47] as a result of the introduction of the transition layer. Note that, apart from the depth ratio ($\hat{d}$), the depth of the transition layer also has played a key role in their investigation. The above problem has also been the focus of Goharzadeh *et al.*,[26] and their experimental observations have confirmed the theoretical predictions by Goyeau *et al.*;[66] that is $\delta_1/D_{gd} \simeq O(1)$, where δ_1 is the thickness of the transition layer and D_{gd} is the grain diameter. Furthermore, their conclusions have agreed with the theoretical predictions by Ochoa-Tapia and Whitaker,[93] namely, $\delta_1/K = O(50)$ (where K denotes the permeability of the porous layer).

Tilton and Cortelezzi[20,21] have examined the linear stability of a single fluid in a porous channel for the cases when porous walls are identical and either one or both the walls are porous (having different permeabilities). Their analysis is for three-dimensional disturbances of arbitrary wave numbers and is based on the modified Orr-Sommerfeld system. Their results have revealed that the role of permeability is to destabilize the flow system. In all the above investigations, the permeability of the porous bottom considered is isotropic and homogeneous. There are many practical scenarios, in which the permeability of the porous layer has directional as well as spatial variations.[22,54–57,64] In view of this, Deepu *et al.*[22,56] have examined the linear stability of horizontal pressure driven flow of a single layer of Newtonian fluid overlying a porous medium with anisotropic and inhomogeneous permeability. They have formulated an eigenvalue problem of the Orr-Sommerfeld type by modelling the porous medium with the Darcy law, modified to account for inhomogeneous and anisotropic permeability effects with an appropriate Beavers-Joseph condition at the liquid-porous interface. The governing system is numerically solved, and the results reveal interesting effects of both anisotropy and inhomogeneous permeabilities on the stability characteristics. They have observed that the modulation of permeability of the porous bottom of the channel provides a potential strategy for controlling the stability of the flow configuration.

Although the relevant literature on such confined flow systems involving the stability of a fluid layer overlying a porous layer at the bottom and a rigid wall on the top is quite rich,[20,21,24,48,50,53,54,58–64] such investigations on instabilities in stratified flows in a porous channel have not been given much attention. The only two studies that the authors have come across are the investigations by Goyal *et al.*[63] (inclined porous channel) and Kumar *et al.*[24] (horizontal porous channel), which are devoted to instabilities in a two-layer Poiseuille/Couette flow overlying a porous medium at the bottom and bounded by a rigid wall at the top, based on Orr-Sommerfeld analysis. They have explored the salient features of different instability modes in the above flow system, by modelling the porous medium as a Darcy-Brinkman porous layer. At the liquid-porous interface, the velocities and the normal stresses are continuous. In addition, the tangential stress at the liquid-porous interface has a jump, and it is proportional to the velocity in the mean flow direction.[65] The proportionality constant or the jump coefficient takes account of the spatial heterogeneity of the liquid-porous interface. Their results for two-layer Poiseuille flow in an inclined porous channel have revealed the coexistence of shear mode at finite wave numbers and interface mode at small wave numbers. There is reduction in frictional resistance on the films due to the presence of the porous layer, and this in turn significantly alters the length and time scales of the shear mode; however, the interface mode is unaffected by this effect.

In the case of a two-layer Couette flow in a horizontal porous channel,[24] they have observed a pair of finite-wave number shear modes in addition to long-wave interface mode of instability, occurring due to the movement of the top wall of the channel and due to the presence of a porous bottom (Darcy-Brinkman).

In the above two studies, the permeability of the porous medium is assumed to be isotropic and homogeneous. This opens up the possibility of exploring the effects of anisotropy and inhomogeneity in the permeability of the porous medium on the stability features of a Poiseuille flow of a viscosity and/or density stratified two-fluid configuration in a porous channel and that is addressed in the present study. The porous channel is bounded by the porous medium with anisotropic and inhomogeneous permeability, saturated with the same fluid as that occupying the lower fluid layer adjacent to it and by a rigid substrate on the top. Thus, the present study is an extension of the analysis by Chang *et al.*[48] to a viscosity-stratified system in a porous channel with anisotropic and inhomogeneous permeability. Furthermore, the study extends the investigation by Deepu *et al.*[56] in a porous channel to a two-layer interface-dominated viscosity-stratified flow system.

The paper is organized as follows: in Sec. II, the physical models along with appropriate boundary conditions at the liquid-liquid interface, at the liquid-porous interface, at the top rigid wall, and at the bottom rigid wall that supports the porous layer are described. The base state velocity profiles are obtained. The details of linear stability analysis are presented in Sec. III and in Sec. IV, and the observed stability characteristics based on the numerical results are presented and discussed. Section V contains the concluding remarks.

II. MATHEMATICAL FORMULATION

We consider a two-dimensional plane Poiseuille flow of two-immiscible, incompressible, Newtonian liquid films with constant density ρ_i and viscosity μ_i (i = 1 in the upper layer and i = 2 in the lower layer; Fig. 1) in a channel bounded by a porous layer of thickness d at the bottom and a rigid wall at the top. The porous medium is saturated by the fluid in the lower layer adjacent to it and is anisotropic and inhomogeneous with constant porosity ϕ. The coordinate system is chosen with the x-axis in the mean flow direction and the y-axis in the vertical direction (Fig. 1). The vertical position is measured from the flat interface between the two fluids in the unperturbed

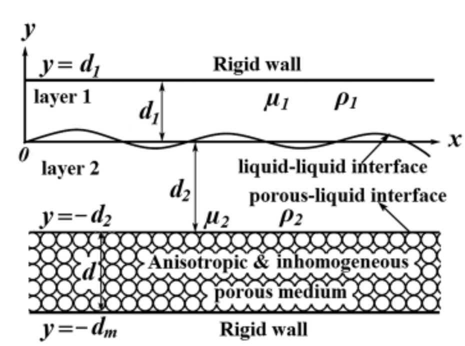

FIG. 1. Schematic of the flow system considered: two-layer Poiseuille flow in a channel bounded by a porous layer supported by a rigid substrate at the bottom and a rigid wall at the top. The two-fluids are viscous, incompressible, and Newtonian fluids having different viscosities and densities. The porous medium has anisotropic and inhomogeneous permeability.

configuration. The thickness of the upper and the lower layers are, respectively, d_1 and d_2.

The continuity and momentum equations in the fluid layers are given by

$$u_{ix} + v_{iy} = 0, \tag{1}$$

$$\rho_i[u_{it} + u_i u_{ix} + v_i u_{iy}] = -p_{ix} + \mu_i[u_{ixx} + u_{iyy}], \tag{2}$$

$$\rho_i[v_{it} + u_i v_{ix} + v_i v_{iy}] = -p_{iy} + \mu_i[v_{ixx} + v_{iyy}], \tag{3}$$

where $0 < y < d_1$ for $i = 1$ and $-d_2 < y < 0$ for $i = 2$. Here (u_i, v_i), $i = 1, 2$ denote the components of velocity along the x and y-directions, respectively, in layers 1 and 2, p_i is the pressure in the fluid layers. The flow in the porous medium ($-d_m < y < -d_2$, where $d_m = d_2 + d$) is governed by the Darcy law, and the governing equations are[56,57]

$$u_{mx} + v_{my} = 0, \tag{4}$$

$$\frac{1}{\phi}u_{mt} = -\frac{1}{\rho_2}p_{mx} - \frac{\mu_2}{\rho_2}\frac{u_m}{K_x\gamma_x(\frac{y}{d})}, \tag{5}$$

$$\frac{1}{\phi}v_{mt} = -\frac{1}{\rho_2}p_{my} - \frac{\mu_2}{\rho_2}\frac{v_m}{K_y\gamma_y(\frac{y}{d})}, \tag{6}$$

where the components $K_x\gamma_x(\frac{y}{d})$ and $K_y\gamma_y(\frac{y}{d})$ of $\vec{\mathbf{K}}$ are the permeabilities along the x and y directions, (u_m, v_m) is the pore-averaged component of fluid velocity in the porous medium, and p_m is the volume average intrinsic pressure in the porous medium.[65]

The above model reduces to that of Chang *et al.*,[48] when the porous medium is isotropic and homogeneous. It is remarked that a two-domain approach has been employed in this study; separate governing equations describe the dynamics in the porous medium (Darcy model) and in the fluid layer (Navier-Stokes equations).

The boundary conditions are

(i) at the bottom of the porous layer:

$$v_m = 0 \quad \text{at} \quad y = -d_m \tag{7}$$

(no penetration at the bottom rigid wall).

(ii) At the top rigid plate:

$$u_1 = 0 \quad \text{at} \quad y = d_1, \tag{8}$$

$$v_1 = 0 \quad \text{at} \quad y = d_1 \tag{9}$$

(no-slip and no-penetration conditions).

(iii) At the material interface of layer 2 and the porous layer, we have Beavers-Joseph conditions[58] given by

$$u_{2y} = \frac{\alpha_{BJ}}{\sqrt{K_x\gamma_x(-\frac{d_2}{d})}}(u_2 - u_m) \quad \text{at} \quad y = -d_2\,, \tag{10}$$

$$v_2 = v_m \quad \text{at} \quad y = -d_2\,, \tag{11}$$

$$p_2 - 2\mu_2 v_{2y} = p_m \quad \text{at} \quad y = -d_2\,, \tag{12}$$

where Eq. (10) is the Beavers-Joseph condition and α_{BJ} is the Beavers-Joseph coefficient.[58,66] The condition (10) accounts for the influence of thickness of the diffusion layer generated near the porous-liquid interface; and following Chen,[94] the component of permeability at the interface along the mean-flow direction is used in the boundary condition (10).

(iv) At the interface between the two-fluids, the conditions are given by

$$u_1 = u_2 \quad \text{at} \quad y = \eta(x,t), \tag{13}$$

$$v_1 = v_2 \quad \text{at} \quad y = \eta(x,t), \tag{14}$$

$$\eta_t = v_1 - u_1\eta_x \quad \text{at} \quad y = \eta(x,t), \tag{15}$$

$$\frac{1}{1+\eta_x^2}[2\mu\eta_x(v_y - u_x) + \mu(u_y + v_x)(1-\eta_x^2)]_1^2 = 0 \quad \text{at} \quad y = \eta(x,t), \tag{16}$$

$$\left[p(1+\eta_x^2) - 2\mu\{\eta_x^2 u_x - (u_y + v_x)\eta_x + v_y\}\right]_1^2 = \frac{-\sigma_0\eta_{xx}}{(1+\eta_x^2)^{\frac{1}{2}}} \quad \text{at} \quad y = \eta(x,t), \tag{17}$$

where $\eta(x, t)$ is the interface vertical deformation around the flat interface position $y = 0$. Equations (13) and (14) correspond to the continuity of components of velocities at the liquid-liquid interface; Eq. (15) is the kinematic boundary condition, and Eqs. (16) and (17) correspond to the balance of shear and normal stresses at the interface. Here, σ_0 is the surface tension at the interface of the two fluid layers.

The steady, fully developed two-layer base flow parallel to the x-direction with flat interface ($y = 0$), over an anisotropic and inhomogeneous porous medium, under constant pressure gradient "P" is governed by

$$\mu_1 u_{1yy} - p_{1x} = 0; \quad p_{1y} = 0 \quad \text{in} \quad 0 \le y \le d_1, \tag{18}$$

$$\mu_2 u_{2yy} - p_{2x} = 0; \quad p_{2y} = 0 \quad \text{in} \quad -d_2 < y \le 0, \tag{19}$$

$$-\frac{1}{\rho_2}p_{mx} - \frac{\mu_2}{\rho_2}\frac{u_m}{K_x\gamma_x(\frac{y}{d})} = 0; \quad p_{my} = 0 \quad \text{in} \quad -(d+d_2) \le y < -d_2, \tag{20}$$

and satisfies

$$u_1 = 0 \quad \text{at} \quad y = d_1, \tag{21}$$

$$u_{2y} = \frac{\alpha_{BJ}}{\sqrt{K_x\gamma_x(-\frac{d_2}{d})}}(u_2 - u_m) \quad \text{at} \quad y = -d_2, \tag{22}$$

$$p_2 = p_m \quad \text{at} \quad y = -d_2, \tag{23}$$

$$u_1 = u_2 \quad \text{at} \quad y = 0, \tag{24}$$

$$[\mu u_y]_1^2 = 0 \quad \text{at} \quad y = 0, \tag{25}$$

$$[p]_1^2 = 0 \quad \text{at} \quad y = 0. \tag{26}$$

The base state solution is given by

$$u_1(y) = \frac{A_1}{2} y^2 + A_2 y + A_3 \quad \text{in} \quad 0 \le y \le d_1, \tag{27}$$

$$u_2(y) = \frac{A_1}{2m} y^2 + \frac{A_2}{m} y + A_3 \quad \text{in} \quad -d_2 < y \le 0, \tag{28}$$

$$u_m(y) = -\frac{A_1}{m} K_x \gamma_x\left(\frac{y}{d}\right) \quad \text{in} \quad -d \le y_m < -d_2, \tag{29}$$

$$p_1 = p_2 = p_m = A_1 \mu_1 x + \text{Constant}, \tag{30}$$

where

$$A_1 = \frac{1}{\mu_1} p_{1x}, \tag{31}$$

$$A_2 = \frac{A_1}{2} \frac{[2\frac{d_2}{m}\sqrt{K_x\gamma_x(-\frac{d_2}{d})} + \alpha_{BJ}\frac{d_2^2}{m} + 2\frac{\alpha_{BJ}}{m}K_x\gamma_x(-\frac{d_2}{d}) - \alpha_{BJ}d_1^2]}{\alpha_{BJ}d_1 + \frac{1}{m}\sqrt{K_x\gamma_x(-\frac{d_2}{d})} + \alpha_{BJ}\frac{d_2}{m}}, \tag{32}$$

$$A_3 = -\frac{A_1 d_1}{2} \frac{A_{3N}}{A_{3D}}, \tag{33}$$

where

$$A_{3N} = \left[2\frac{d_2}{m}\sqrt{K_x\gamma_x(-\frac{d_2}{d})} + \alpha_{BJ}\frac{d_1 d_2}{m} + \frac{d_1}{m}\sqrt{K_x\gamma_x(-\frac{d_2}{d})}\right] + \left[2\frac{\alpha_{BJ}}{m}K_x\gamma_x(-\frac{d_2}{d}) + \alpha_{BJ}\frac{d_2^2}{m}\right],$$

$$A_{3D} = \alpha_{BJ}d_1 + \frac{1}{m}\sqrt{K_x\gamma_x(-\frac{d_2}{d})} + \alpha_{BJ}\frac{d_2}{m},$$

and $m = \frac{\mu_2}{\mu_1}$ is the ratio of viscosity of fluids in the two layers. For a given streamwise pressure gradient, $u_m(y)$ is dependent on the permeability of the porous medium. In the absence of the lower layer close to the porous medium (layer 2) and with $m = 1$, the above coefficients A_1, A_2, and A_3 reduce to those in Eq. (2.9) of Deepu *et al.*[56]

The governing equations and the boundary conditions in dimensionless form are obtained using the following scales:

$$x^* = \frac{x}{d_1}, y^* = \frac{y}{d_1}, t^* = \frac{tU}{d_1}, u_1^* = \frac{u_1}{U}, v_1^* = \frac{v_1}{U}, \quad u_2^* = \frac{u_2}{U}, v_2^* = \frac{v_2}{U}, p_1^* = \frac{p_1}{\rho_1 U^2}, \tag{34}$$

$$p_2^* = \frac{p_2}{\rho_1 U^2}, \eta^* = \frac{\eta}{d_1}, x_m^* = \frac{x}{d}, y_m^* = \frac{y}{d}, t_m^* = \frac{tV_m}{d}, \quad p_m^* = \frac{p_m d}{\mu_2 V_m}, u_m^* = \frac{u_m}{V_m}, v_m^* = \frac{v_m}{V_m}, \tag{35}$$

where U is the velocity of the unperturbed fluid 1-fluid 2 interface ($U = u_1{-}_{y=0} = u_2{-}_{y=0}$) and $V_m = u_m|_{y=-d_2}$ is the velocity in the porous medium at the porous-liquid interface and are given by

$$U = A_3 = -\frac{A_1 d_1^2}{2} \frac{[n + n^2 + \frac{\delta\hat{d}}{\alpha_{BJ}}\sqrt{\gamma_x(\frac{-n}{\hat{d}})} + \frac{2}{\alpha_{BJ}}n\delta\hat{d}\sqrt{\gamma_x(\frac{-n}{\hat{d}})} + 2\delta^2\hat{d}^2\gamma_x(\frac{-n}{\hat{d}})]}{m + n + \frac{\delta\hat{d}}{\alpha_{BJ}}\sqrt{\gamma_x\left(\frac{-n}{\hat{d}}\right)}}, \tag{36}$$

$$V_m = -\frac{A_1 d_1^2}{m}\delta^2\hat{d}^2\gamma_x\left(\frac{-n}{\hat{d}}\right), \tag{37}$$

and $n = \frac{d_2}{d_1}$, $\delta = \frac{\sqrt{K_x}}{d}$, and $\hat{d} = \frac{d}{d_1}$ (the depth ratio of the porous layer thickness to the thickness of the upper layer). In terms of the dimensionless variables (after suppressing $*$), the governing equations are given by

$$\nabla \cdot \vec{\boldsymbol{u}}^{(1)} = 0, \tag{38}$$

$$\frac{\partial \vec{\boldsymbol{u}}^{(1)}}{\partial t} + (\vec{\boldsymbol{u}}^{(1)} \cdot \nabla)\vec{\boldsymbol{u}}^{(1)} = -\nabla p_1 + \frac{1}{Re}\nabla^2 \vec{\boldsymbol{u}}^{(1)} \tag{39}$$

in layer 1 ($0 < y < 1$), and

$$\nabla \cdot \vec{\boldsymbol{u}}^{(2)} = 0, \tag{40}$$

$$\frac{\partial \vec{\boldsymbol{u}}^{(2)}}{\partial t} + (\vec{\boldsymbol{u}}^{(2)} \cdot \nabla)\vec{\boldsymbol{u}}^{(2)} = -\frac{1}{r}\nabla p_2 + \frac{m}{r\mathrm{Re}}\nabla^2 \vec{\boldsymbol{u}}^{(2)} \tag{41}$$

in layer 2 ($-n < y < 0$), where $\vec{\boldsymbol{u}}^{(1)} = (u_1, v_1)$, p_1 and $\vec{\boldsymbol{u}}^{(2)} = (u_2, v_2)$, p_2 denote the dimensionless velocities and pressure distributions in the upper and lower layers, respectively, and $r = \frac{\rho_2}{\rho_1}$ is the ratio of densities in the two layers.

In this study, vertical variations of inhomogeneity of the porous medium in both the horizontal and vertical directions have been considered to be the same.[57,95] This is based on the model for a practical scenario described by Chen.[94] The ratio $\frac{K_x}{K_y}(= \xi)$ describes the anisotropy of the permeability of the porous medium. A reduction in ξ corresponds to an increase in permeability in the y-direction, and this causes reduction in flow resistance. In this study, ξ ranges from its limiting value for the porous layer with nearly vanishing horizontal permeability ($\xi = 10^{-4}$) to a value $\xi = 3$ that exceeds that for the isotropic case ($\xi = 1$).

In the porous layer $-(n + \hat{d}) < y < -n$ or $-\frac{(n+\hat{d})}{\hat{d}} < y_m < -\frac{n}{\hat{d}}$, we have

$$\boldsymbol{\nabla}_m \cdot \vec{\boldsymbol{u}}_m = 0, \tag{42}$$

$$\frac{Re_m}{\phi}\frac{\partial \vec{\boldsymbol{u}}_m}{\partial t_m} = -\boldsymbol{\nabla}_m p_m - \frac{\vec{\boldsymbol{a}}}{\delta^2}, \tag{43}$$

where $\vec{\boldsymbol{u}}_m = (u_m, v_m)$, p_m denote the dimensionless velocities and pressure distributions in the porous medium, respectively. Here,

$$\vec{\boldsymbol{a}} = \left(\frac{u_m}{\gamma_x(y_m)}, \frac{\xi v_m}{\gamma_y(y_m)}\right), \gamma_x(y_m) = \gamma_y(y_m) = e^{A(\frac{n+\hat{d}}{\hat{d}} + y_m)}.$$

Note that $y = \hat{d}y_m$. The inhomogeneous permeability is unity at the bottom ($y_m = -\frac{(n+\hat{d})}{\hat{d}}$) and increases with y_m when A is positive and decreases with y_m when A is negative. The value of A ranges from zero (in homogeneous case) to a non-zero value between -5 and 5 for an inhomogeneous porous medium.[22,94] Positive and negative values of A, respectively, correspond to an increase and a decrease in permeabilities in the x and y directions. The effects of the degree of inhomogeneity along the depth of the porous layer on the stability characteristics of the system is analysed by varying the parameter A. It is important to note that while variation in the mean permeability is captured by the variations in the Darcy number, the variations in A capture the inhomogeneous modulations of permeability along the depth of the porous layer.

The boundary conditions in dimensionless variables are

$$v_m = 0 \quad \text{at} \quad y_m = -\frac{(n + \hat{d})}{\hat{d}} \quad \text{or} \quad y = -(n + \hat{d}), \tag{44}$$

$$u_1 = 0 \quad \text{at} \quad y = 1, \tag{45}$$

$$v_1 = 0 \quad \text{at} \quad y = 1, \tag{46}$$

$$u_{2y} = \frac{\alpha_{BJ}}{\hat{d}\delta\sqrt{\gamma_x(-\frac{n}{\hat{d}})}}\left[u_2 - \frac{mRe_m}{r\hat{d}\mathrm{Re}}u_m\right] \quad \text{at} \quad y_m = -\frac{n}{\hat{d}} \quad \text{or} \quad y = -n, \tag{47}$$

$$v_2 = \frac{mRe_m}{r\hat{d}\mathrm{Re}}v_m \quad \text{at} \quad y_m = -\frac{n}{\hat{d}} \quad \text{or} \quad y = -n, \tag{48}$$

$$p_2 - \frac{2m}{\mathrm{Re}}v_{2y} = \frac{m^2 Re_m}{r\mathrm{Re}^2}\frac{p_m}{\hat{d}^2} \quad \text{at} \quad y_m = -\frac{n}{\hat{d}} \quad \text{or} \quad y = -n, \tag{49}$$

$$u_1 = u_2 \quad \text{at} \quad y = \eta(x, t), \tag{50}$$

$$v_1 = v_2 \quad \text{at} \quad y = \eta(x, t), \tag{51}$$

$$\eta_t = v_1 - u_1\eta_x \quad \text{at} \quad y = \eta(x, t), \tag{52}$$

$$m\left[(1 - \eta_x^2)(u_{2y} + v_{2x}) - 4\eta_x u_{2x}\right] - \left[(1 - \eta_x^2)(u_{1y} + v_{1x}) - 4\eta_x u_{1x}\right] = 0 \quad \text{at} \quad y = \eta(x, t), \tag{53}$$

$$\left[p_2(1 + \eta_x^2) - \frac{2m}{\mathrm{Re}}(\eta_x^2 u_{2x} - (u_{2y} + v_{2x})\eta_x + v_{2y})\right] - \left[p_1(1 + \eta_x^2) - \frac{2}{\mathrm{Re}}(\eta_x^2 u_{1x} - (u_{1y} + v_{1x})\eta_x + v_{1y})\right] = -\frac{S\eta_{xx}}{\sqrt{1 + \eta_x^2}} \quad \text{at} \quad y = \eta(x, t). \tag{54}$$

The flow is governed by the following dimensionless parameters:

$Re = \frac{\rho_1 d_1 U}{\mu_1}$ (the Reynolds number in the fluid layers), $Re_m = \frac{\rho_2 d V_m}{\mu_2}$ (the Reynolds number in the porous layer), $\delta = \frac{\sqrt{K_x}}{d}$ (the permeability parameter or the Darcy number), and $S = \frac{\sigma_0}{\rho_1 d_1 U^2}$ (the surface tension parameter). We note that $\frac{V_m}{U} = \frac{m}{r\hat{d}}\frac{Re_m}{\mathrm{Re}}$.

The dimensionless base flow is given by

$$U_{1B} = 1 + C_2 y + C_1 y^2, \tag{55}$$

$$U_{2B} = 1 + \frac{C_2}{m}y + \frac{C_1}{m}y^2, \tag{56}$$

$$U_{mB} = \frac{\gamma_x(y_m)}{\gamma_x(-\frac{n}{\hat{d}})}, \tag{57}$$

$$P_{1B} = P_{2B} = P_{mB} = -\frac{2}{\mathrm{Re}}\frac{m + n + \frac{\delta\hat{d}}{\alpha_{BJ}}\sqrt{\gamma_x(\frac{-n}{\hat{d}})}}{[n + n^2 + \frac{\delta\hat{d}}{\alpha_{BJ}}\sqrt{\gamma_x(\frac{-n}{\hat{d}})} + \frac{2}{\alpha_{BJ}}n\delta\hat{d}\sqrt{\gamma_x(\frac{-n}{\hat{d}})} + 2\delta^2\hat{d}^2\gamma_x(\frac{-n}{\hat{d}})]} + \text{Constant}, \tag{58}$$

where

$$C_1 = -\frac{[m + n + \frac{\delta\hat{d}}{\alpha_{BJ}}\sqrt{\gamma_x(\frac{-n}{\hat{d}})}]}{[n + n^2 + \frac{\delta\hat{d}}{\alpha_{BJ}}\sqrt{\gamma_x(\frac{-n}{\hat{d}})} + \frac{2}{\alpha_{BJ}}n\delta\hat{d}\sqrt{\gamma_x(\frac{-n}{\hat{d}})} + 2\delta^2\hat{d}^2\gamma_x(\frac{-n}{\hat{d}})]}, \tag{59}$$

$$C_2 = -\frac{[-m + n^2 + 2\frac{n\delta\hat{d}}{\alpha_{BJ}}\sqrt{\gamma_x(\frac{-n}{\hat{d}})} + 2\delta^2\hat{d}^2\gamma_x(\frac{-n}{\hat{d}})]}{[n + n^2 + \frac{\delta\hat{d}}{\alpha_{BJ}}\sqrt{\gamma_x(\frac{-n}{\hat{d}})} + \frac{2}{\alpha_{BJ}}n\delta\hat{d}\sqrt{\gamma_x(\frac{-n}{\hat{d}})} + 2\delta^2\hat{d}^2\gamma_x(\frac{-n}{\hat{d}})]}. \tag{60}$$

Note that U_{mB} is constant and takes the value 1, when the porous medium is homogeneous (A = 0).

The base state velocity profiles (U_{iB}, $i = 1, 2$ in fluid layers) for stationary flows in a two-layer configuration are presented as a function of y for different depth ratios ($\hat{d} = 1, 5, 10$) of the homogeneous (A = 0) and isotropic ($\xi = 1$) porous bottom with permeability $\delta = 0.002$ in Figs. 2(a) and 2(b). In a configuration with a low viscous fluid in a thinner layer close to the porous bottom [$m = 0.8$ and $n = 0.5$, Fig. 2(a)], an increase in the depth ratio $\hat{d}$ decreases (increases) the base velocity at the thicker upper layer (thinner lower layer). The above conclusions remain the same as the viscosity-stratification is reversed ($m = 1.5$) and $n = 2$ [Fig. 2(b)]. Note that the maximum base velocity occurs in the upper (lower) fluid layer for a flow system with $m = 0.8$ and $n = 0.5$ ($m = 1.5$ and $n = 2$). This happens at the smallest (largest) $\hat{d}$ considered in Fig. 2(a) [Fig. 2(b)]. The streamwise velocity experiences a jump discontinuity atc the liquid-porous interface, and it is consistent with the Beavers-Joseph[58] condition at this interface, which relates the relative velocity at the interface with the shear stress. As velocities are not scaled with the same quantities in the fluid layers and in the porous medium, the base velocity in the porous

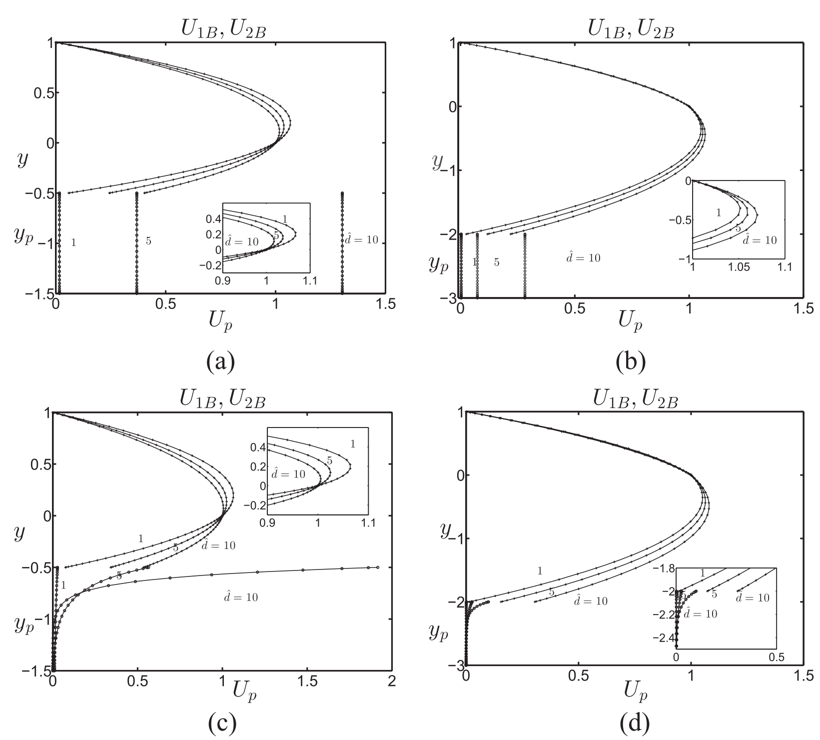

FIG. 2. Base flow profiles for different porous layer thicknesses ($\hat{d}$) when other parameters are $\alpha_{BJ} = 0.1$, $\phi = 0.3$, $r = 1$, $S = 0.1$, $\delta = 0.002$, and $\hat{d} = 1, 5, 10$, (a) $m = 0.8$, $n = 0.5$, $A = 0$, (b) $m = 1.5$, $n = 2$, $A = 0$, (c) $m = 0.8$, $n = 0.5$, $A = 1$, and (d) $m = 1.5$, $n = 2$, $A = 1$. The velocity in the porous layer is scaled with the quantity V_m/U, that is, $U_m = u_m V_m/U$. Here, $y_p = (y_m + n)/\hat{d} - n$ and $U_p = U_{mB}(V_m/U)10^3$.

medium had to be rescaled to be comparable with velocities in the fluid layers. That is why, in the porous medium, the base velocity corresponding to $U_{mB}(V_m/U)10^3$ is plotted as a function of $(((y_m + n)/\hat{d}) - n)$ to normalise the porous medium depth, where U_{mB} is given by Eq. (57). As a result of this scaling, the base velocity in the porous layer is constant for each $\hat{d}$. Note that the scaling is used only for plotting the base state profiles in the porous layer and not in the subsequent stability analysis. At any $\hat{d}$, the base state velocity decreases in the porous layer with a decrease in permeability δ (figure not shown).

When the porous medium is isotropic and homogeneous, the velocity in the porous medium increases with an increase in $\hat{d}$ [Figs. 2(a) and 2(b)], the presence of inhomogeneity reduces the porous layer velocity to values which are negligibly small [Figs. 2(c) and 2(d)]. The velocity in the porous layer is larger, when a thinner layer hosting a less viscous fluid is adjacent to the porous medium [Figs. 2(a) and 2(c)], both in the presence and absence of inhomogeneity.

In what follows, a linear temporal stability of the above stationary flow is investigated within the framework of Orr-Sommerfeld analysis.

III. LINEAR STABILITY ANALYSIS

The linear stability of the base flow to infinitesimal disturbances is analysed by considering two-dimensional perturbations

$$\text{flow variable} = \text{base state} + \text{perturbation}\,\tilde{f}$$

and applying normal mode expansion to the perturbed variable in the fluid layers as $\tilde{f} = \hat{f}(y)e^{i\alpha(x-ct)}$, and in the porous layer $\tilde{f}_m = \hat{f}_m(y)e^{i\alpha_m(x_m-c_mt_m)}$. Here, α is the streamwise wave number of the disturbance, $c = c_r + ic_i$ is the complex phase speed, c_r is the wave speed, and c_i is the time growth rate. Here $\hat{f}(y)$ and $\hat{f}_m(y)$ represent the amplitude of the perturbations of the variables in the liquid layers and porous layer, respectively. Note that

$$\alpha = \hat{d}\alpha_m,\ c = \frac{m}{r\hat{d}}\frac{Re_m}{Re}c_m,\ x = \hat{d}x_m,$$
$$t = \frac{r}{m}\hat{d}^2\frac{Re}{Re_m}t_m,\ \alpha(x-ct) = \alpha_m(x_m - c_mt_m).$$

Substituting these in the linearized governing equations and in the boundary conditions and following the standard procedure, the modified Orr-Sommerfeld system of equations is obtained[96] and is given by

$$(D^2-\alpha^2)^2\phi_1 = i\alpha Re[(U_{1B}-c)(D^2-\alpha^2)\phi_1 - (D^2U_{1B})\phi_1],\ 0<y<1, \tag{61}$$

$$m(D^2-\alpha^2)^2\phi_2 = ir\alpha Re[(U_{2B}-c)(D^2-\alpha^2)\phi_2 - (D^2U_{2B})\phi_2],\ -n<y<0, \tag{62}$$

$$\begin{aligned}&\frac{Re_m}{\phi}i\alpha_mc_m(D_m^2-\alpha_m^2)\phi_m\\ &\quad= -\frac{\xi}{\delta^2}\frac{\alpha_m^2\phi_m}{\gamma_y(y_m)} + \frac{D_m^2\phi_m}{\delta^2\gamma_x(y_m)} - \frac{(D_m\phi_m)(D_m\gamma_x)}{\delta^2\gamma_x^2(y_m)},\\ &\quad -\frac{(n+\hat{d})}{\hat{d}} < y_m < -\frac{n}{\hat{d}},\end{aligned} \tag{63}$$

$$\phi_m = 0 \quad \text{at} \quad y_m = -\frac{(n+\hat{d})}{\hat{d}}, \tag{64}$$

$$D\phi_1 = 0 \quad \text{at} \quad y = 1, \tag{65}$$

$$\phi_1 = 0 \quad \text{at} \quad y = 1, \tag{66}$$

$$D^2\phi_2 = \frac{\alpha_{BJ}}{\hat{d}\delta\sqrt{\gamma_x(-\frac{n}{\hat{d}})}}\left[D\phi_2 - \frac{Re_m}{Re\,\hat{d}}\frac{m}{r}(D_m\phi_m)\right] \quad \text{at} \quad y_m = -\frac{n}{\hat{d}}, \tag{67}$$

$$\phi_2 = \frac{m\,Re_m}{r\,Re}\phi_m \quad \text{at} \quad y_m = -\frac{n}{\hat{d}}, \tag{68}$$

$$\begin{aligned}&-DU_{2B}(2-r)i\alpha\phi_2 + 3\alpha^2\frac{m}{Re}D\phi_2 - \frac{m}{Re}D^3\phi_2\\ &+ i\alpha rD\phi_2(U_{2B}-c) + \frac{m\,Re_m}{\phi\,Re}\frac{i\alpha c}{\hat{d}}(D_m\phi_m)\\ &-\frac{m^2Re_m}{rRe^2}\frac{1}{\hat{d}^3}\frac{D_m\phi_m}{\delta^2\gamma_x(y_m)} = 0 \quad \text{at} \quad y_m = -\frac{n}{\hat{d}},\end{aligned} \tag{69}$$

$$m[D\phi_2 - D\phi_1] = hC_2(m-1) \quad \text{at} \quad y = 0, \tag{70}$$

$$\phi_2 = \phi_1 \quad \text{at} \quad y = 0, \tag{71}$$

$$m[D^2\phi_2 + \alpha^2\phi_2] - [D^2\phi_1 + \alpha^2\phi_1] = 0 \quad \text{at} \quad y = 0, \tag{72}$$

$$\begin{aligned}&i\alpha\,Re[(U_{1B}-c)D\phi_1 - C_2\phi_1] - i\alpha\,Re\,r\left[(U_{2B}-c)D\phi_2 - \frac{C_2}{m}\phi_2\right]\\ &+ m(D^3\phi_2 - 3\alpha^2D\phi_2) - (D^3\phi_1 - 3\alpha^2D\phi_1)\\ &= i\alpha^3SRe\,h \quad \text{at} \quad y = 0,\end{aligned} \tag{73}$$

$$\phi_1 + h(U_{1B}-c) = 0 \quad \text{at} \quad y = 0, \tag{74}$$

where ϕ_1, ϕ_2, and ϕ_m denote the amplitudes of the stream function perturbations in layer 1, layer 2, and porous layer, respectively, h is the disturbance amplitude in deflection of the fluid-fluid interface, $D = \frac{d}{dy}$, $D_m = \frac{d}{dy_m}$, and $y = \hat{d}y_m$. In the limit $m = 1$, $n = 1$, and $r = 1$ with $A \neq 0$ and $\xi \neq 1$, the above equations and the boundary conditions reduce to those of Deepu *et al.*[56] for the stability of Poiseuille flow of a single fluid in a channel bounded by anisotropic and inhomogeneous porous medium at the bottom and a rigid wall at the top. When A = 0 and ξ = 1, Eqs. (61)–(74) reduce to those of Chang *et al.*,[48] by taking into account the different velocity scale chosen by them. In the absence of the porous medium at the bottom, we recover the Orr-Sommerfeld system obtained by Yiantsios and Higgins,[3] for the linear stability of two-layer Poiseuille flow in a rigid channel.

IV. RESULTS AND DISCUSSION

The coupled linear stability problem governed by (61)–(74) is solved numerically using the Chebyshev spectral collocation method[96] for infinitesimal disturbances of arbitrary wave numbers. Each perturbation amplitude function $\phi_1(y)$, $\phi_2(y)$, and $\phi_m(y)$ is approximated using a truncated Chebyshev expansion (in terms of Chebyshev polynomials)

$$\phi_1 = \sum_{l=0}^{N} A_l T_l(y), \phi_2 = \sum_{l=0}^{N} B_l T_l(y), \phi_m = \sum_{l=0}^{N} C_l T_l(y_m) \quad (75)$$

and is substituted in the Orr-Sommerfeld system (61)–(63). Here A_l, B_l, and C_l are unknowns to be determined. The functions are then evaluated at the Gauss-Lobatto points $y_j = \cos(\frac{\pi j}{N}), j = 0, 1, 2, 3, \ldots, N$.[96] This results in the generalized eigenvalue problem

$$\mathcal{A}^{*}\boldsymbol{x} = c\mathcal{B}^{*}\boldsymbol{x} \quad (76)$$

for the eigenvalues (c, c_m) and eigenvector $\boldsymbol{x} = (\phi_1(y), h, \phi_2(y), \phi_m(y))$, where $\mathcal{A}^*$ and $\mathcal{B}^*$ are $(3N + 4) \times (3N + 4)$ matrices and $\boldsymbol{x}$ is a $(3N + 4) \times 1$ vector.

For a given N, the relative error (E_N) is defined by

$$E_N = \frac{||\mathbf{c}_{N+1} - \mathbf{c}_N||_2}{||\mathbf{c}_N||_2},$$

where $||\cdot||_2$ is the L_2-norm.[20,23] Here, the components of the vectors $\mathbf{c}_N$ and $\mathbf{c}_{N+1}$ are the eigenvalues corresponding to the twenty least stable modes of the eigenvalue problem (76), obtained using N and N + 1 Chebyshev polynomials, respectively, in each layer. The number of Chebyshev polynomials (N) required to resolve the problem accurately is determined. The convergence of the eigenvalues with different N is checked. In all the computations, the porosity parameter ϕ is taken as 0.3.

Figure 3 show the relative error, E_N, as a function of the number of Chebyshev polynomials (N) employed in the computations, for an isotropic (ξ = 1) and homogeneous (A = 0) porous bottom, when $m = 1.5$, $n = 2$, $\alpha_{BJ} = 0.1$, $\phi = 0.3$, $r = 1$, and $S = 0.1$ for different depth ratios $\hat{d}$ and Darcy numbers δ. We observe that the relative error of the order 10^{-6} is achieved for permeabilities of the order of 0.0002–0.002 with N ≥ 110 polynomials and there is no significant change in the above conclusions with a decrease in the depth ratio $\hat{d}$. In the case of anisotropic ($\xi \neq 1$) and inhomogeneous (A ≠ 1) porous medium, Fig. 4 shows that the accuracy of order 10^{-6} is attained with N ≥ 100. Hence, the computations are performed for each case with the minimum N required for convergence of the order of 10^{-6}.

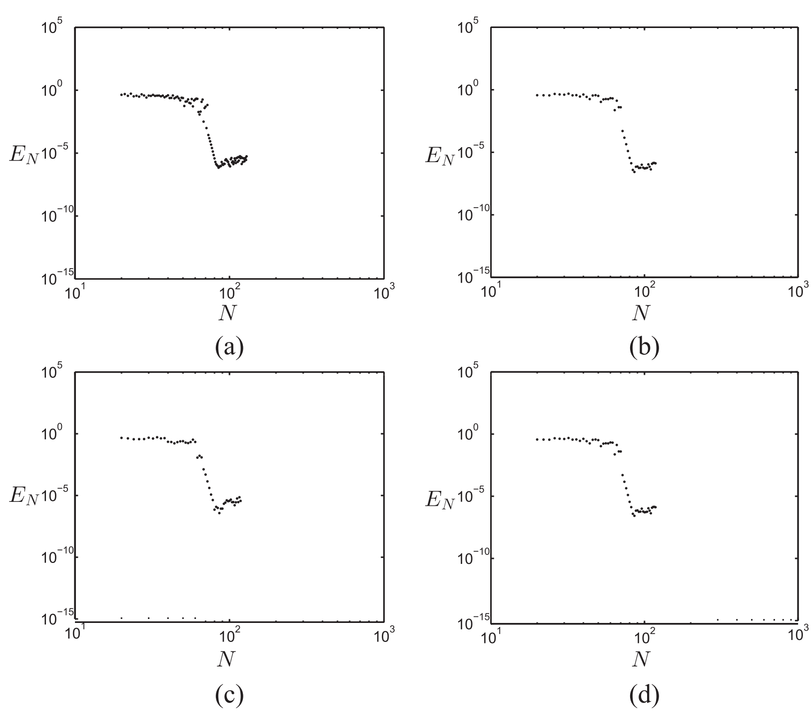

FIG. 3. The relative error E_N as a function of the Chebyshev collocation number N. The other parameters are $m = 1.5$, $n = 2$, $\alpha_{BJ} = 0.1$, $\phi = 0.3$, $r = 1$, $S = 0.1$, $A = 0$, and $\xi = 1$, (a) $\hat{d} = 5$, $\delta = 0.0002$, (b) $\hat{d} = 10$, $\delta = 0.0002$, (c) $\hat{d} = 5$, $\delta = 0.002$, and (d) $\hat{d} = 10$, $\delta = 0.002$.

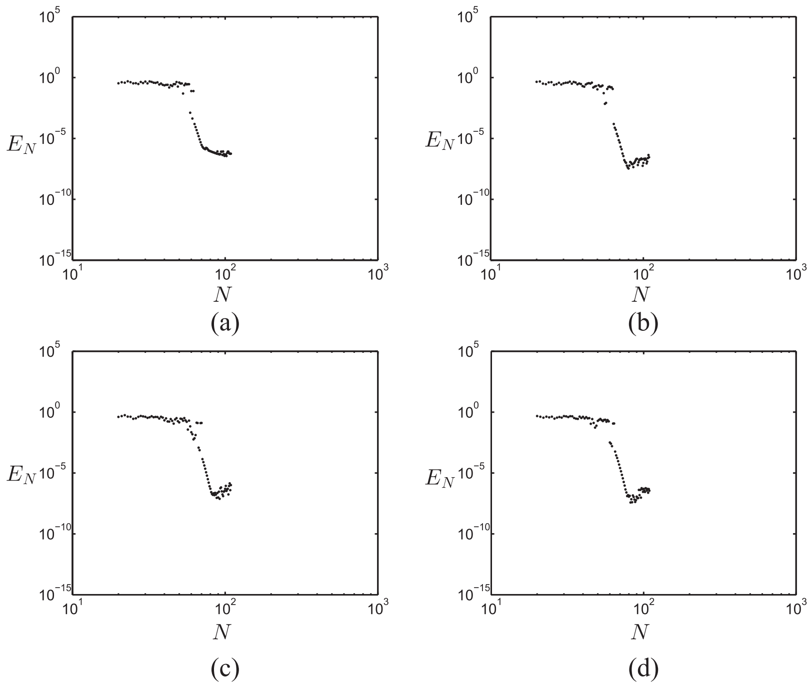

FIG. 4. The relative error E_N as a function of the Chebyshev collocation number N. The other parameters are m = 1.5, n = 2, α_{BJ} = 0.1, ϕ = 0.3, r = 1, S = 0.1, and δ = 0.002, (a) $\hat{d}$ = 10, ξ = 3, A = 0, (b) $\hat{d}$ = 10, ξ = 3, A = 1, (c) $\hat{d}$ = 5, ξ = 1, A = 1, and (d) $\hat{d}$ = 10, ξ = 1, A = 1.

The correctness of the developed code is also assessed by validating the results obtained in the limiting cases for a single layer Poiseuille flow (a) confined between anisotropic/isotropic and homogeneous/inhomogeneous porous bottom and rigid top (critical Reynolds numbers[56]), (b) for isotropic and homogeneous porous bottom and rigid top (spectral results[48]), and (c) for a two-layer Poiseuille flow in a rigid channel (spectral results[3]) and the results are in good agreement (Tables I and II) for α_{BJ} = 0.1 and porosity ϕ = 0.3.

The presence of the porous bottom alters the velocity profile (base state) as the parameters describing the porous medium are varied (see base state profiles, Fig. 2) and therefore influences the stability results; furthermore, it introduces nonzero disturbance velocities at the porous-liquid layer 2 interface; in addition, due to viscosity-stratification, there are perturbations at the interface of the two immiscible layers. We examine the effects of these perturbations on the stability properties as the anisotropy parameter (ξ), the inhomogeneity

TABLE I. Comparison of eigenvalues in the limiting cases when α_{BJ} = 0.1 and porosity ϕ = 0.3.

Description	Parameter values	Eigenvalues available	Computed eigenvalues
Single layer Poiseuille flow overlying a homogeneous, isotropic porous layer at the bottom and a rigid top[48]	$Re = 10^4$, $\alpha = 1$, $\hat{d} = 10$, $\delta = 0.001$	$c = c_r + ic_i = 0.479\,424\,76 + i0.032\,748\,67$	$0.479\,352\,98 + i0.032\,668\,49$
Two-layer Poiseuille flow in a rigid channel[3]	$m = 5$, $S = 0.1$, $Re = 1$, $\alpha = 10$	$0.999\,98 - i0.008\,199$	$0.999\,98 - i0.008\,198$

TABLE II. Comparison of critical Reynolds numbers in the limiting cases (m = 1, n = 1) in the limiting cases when α_{BJ} = 0.1 and porosity ϕ = 0.3.

Description	Parameter values	Critical Re available	Computed critical Re
Single layer Poiseuille flow overlying an anisotropic, homogeneous porous medium at the bottom and a rigid top[56]	$\xi = 3$, $A = 0$, $\hat{d} = 10$, $\delta = 0.002$	4795	4799
Single layer Poiseuille flow overlying an isotropic, inhomogeneous porous medium at the bottom and a rigid top[56]	$\xi = 1$, $A = 1$, $\hat{d} = 10$, $\delta = 0.002$	2866	2807

parameter (A), the depth ratio ($\hat{d}$), and the Darcy number (δ) are varied.

Our preliminary computations performed for a wide range of all parameters governing the system have revealed the coexistence of different types of modes (porous mode, interface mode, fluid layer mode, and shear mode) and coalescence of the modes in different bandwidths of wave numbers and low to high Reynolds numbers.

Furthermore, there are a number of dimensionless parameters governing the stability characteristics. As a result, the presentation of the results about different unstable modes becomes cumbersome and complicated; so we have restricted the discussions to porous mode and interface mode and we have only made a mention of the occurrence of the other modes with no further details and have postponed the discussion to our future study.

In the following, we have focused on the stability characteristics of two-dimensional disturbances of the base state of two-layer Poiseuille flow in a channel bounded by an inhomogeneous, anisotropic porous bottom and a rigid top.

A. Two-layer flow in a channel with homogeneous, isotropic/anisotropic porous bottom and rigid top

The spectral results obtained through the numerical computations are presented in Figs. 5(a) and 5(b), when a high viscous fluid (m = 1.5) occupies a thicker (n = 2) layer adjacent to the porous medium with isotropic (ξ = 1) and homogeneous (A = 0) permeability. At Re = 3000, $\hat{d}$ = 10, and δ = 0.01, for a lower wave number α = 0.2, an unstable mode with c_r < 1 emerges [Fig. 5(b)]; an increase in α to α = 0.75 shifts the dominant unstable mode to one with c_r > 1 [Fig. 5(a)]. When inhomogeneous permeability effects are incorporated (A = 1), then two unstable modes: one with c_r < 1 and the other with c_r > 1 emerge at α = 0.6, when Re = 10 000 and δ = 0.002 [Fig. 5(d)]. The occurrence of these modes may be associated with the presence of viscosity-stratification and the presence of the porous medium as a lower channel wall. In the reverse arrangement of the flow system (m = 0.8, n = 0.5), the unstable mode with c_r < 1 alone exists [Fig. 5(c)]. The other parameters in Fig. 5 are fixed as $\hat{d}$ = 10, α_{BJ} = 0.1, ϕ = 0.3, r = 1, S = 0.1, ξ = 1. It is to be noted that an increase in ξ reduces the growth rate of the unstable mode (figure not shown).

The growth rates as a function of wave number for different values of δ [Figs. 6(a) and 6(b)], $\hat{d}$ [Figs. 6(c) and 6(d)], and ξ [Figs. 6(e) and 6(f)] are presented for a configuration with isotropic (ξ = 1)/anisotropic ($\xi \neq 1$) and homogeneous (A = 0) porous bottom. Figure 6(a) reveals that there is an unstable mode in a window of moderate to O(1) wave numbers for each δ considered and the maximum growth rate is non-monotonic as the permeability parameter δ increases. As this mode exists in this window of wave numbers for any permeability considered for the two-layer configuration, we refer to this mode as the interface mode.[3]

Simultaneously, there exists another mode with a negative growth rate at smaller permeability [δ = 0.0002 Fig. 6(b)] of the homogeneous porous bottom. An increase in δ (δ = 0.002) gives rise to a dispersion curve with two humps,

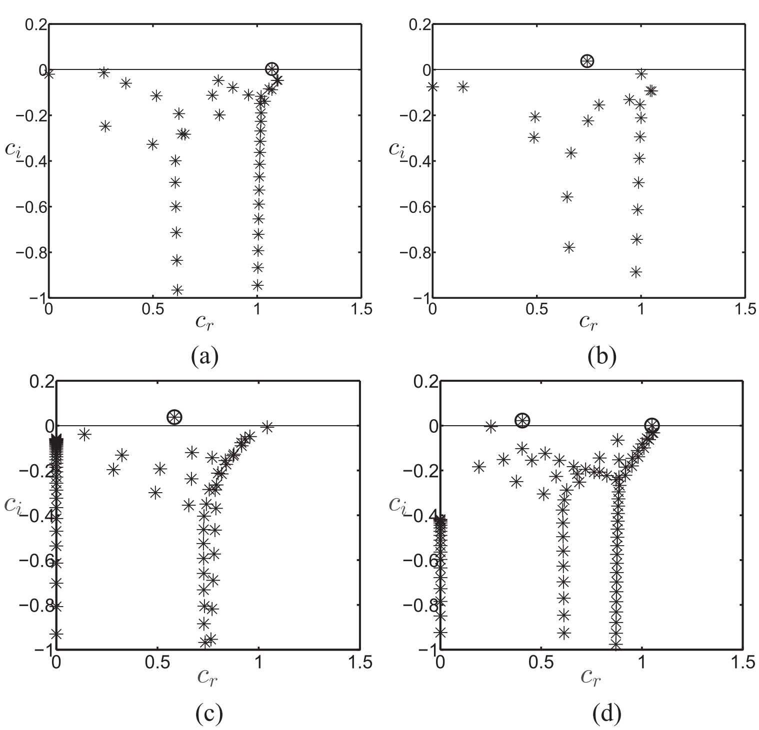

FIG. 5. Spectral results for an isotropic porous bottom (ξ = 1) with porosity ϕ = 0.3, when α_{BJ} = 0.1, S = 0.1, r = 1, and $\hat{d}$ = 10. The influence of viscosity-stratification and inhomogeneity in permeability of the porous medium is presented for (a) m = 1.5, n = 2, δ = 0.01, Re = 3000, α = 0.75, A = 0, (b) m = 1.5, n = 2, δ = 0.01, Re = 3000, α = 0.2, A = 0, (c) m = 0.8, n = 0.5, δ = 0.002, Re = 10 000, α = 0.6, A = 1, and (d) m = 1.5, n = 2, δ = 0.002, Re = 10 000, α = 0.6, A = 1.

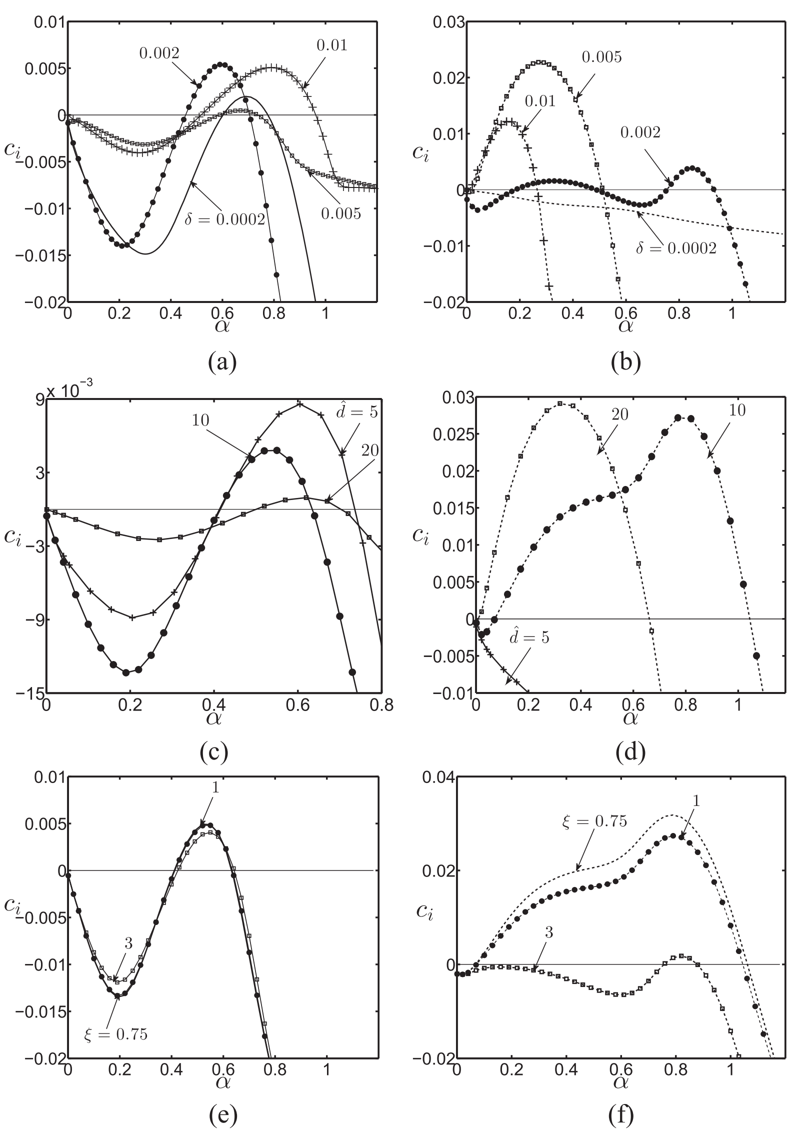

FIG. 6. Dispersion curves for different δ [(a) and (b)], $\hat{d}$ [(c) and (d)], and ξ [(e) and (f)] for the first two unstable modes with the other parameters as m = 1.5, n = 2, α_{BJ} = 0.1, ϕ = 0.3, r = 1, S = 0.1, and A = 0, (a) interface mode (solid lines), (b) porous mode (dashed lines), δ = 0.0002 (no symbol), δ = 0.002 (filled circles), δ = 0.005 (squares), and δ = 0.01 (plus) at Re = 6000 and $\hat{d} = 10$, ξ = 1, (c) interface mode (solid lines), (d) porous mode (dashed lines), $\hat{d} = 5$ (no symbol), $\hat{d} = 10$ (filled circles), $\hat{d} = 20$ (squares) at Re = 10 000 and δ = 0.002, ξ = 1, (e) interface mode (solid lines), and (f) porous mode (dashed lines), ξ = 0.75 (no symbol), ξ = 1 (filled circles), and ξ = 3 (squares) at Re = 10 000 and $\hat{d} = 10$, δ = 0.002.

exhibiting positive growth rate, one close to the short wavelength regime [wave number closer to O(1)] and the other in the long wavelength regime. Of the two local maxima, the one in the short wave regime exhibits a global maximum. With a further increase in δ (δ = 0.005), the two hump structure in the dispersion curve disappears and becomes a single hump structure, stabilizing short wave modes. This single hump is in the long wave regime, having a higher growth rate. This mode is referred to as a porous mode.[23] A non-monotonic behaviour is observed as δ is increased to δ = 0.01, destabilizing the long waves and the growth rate is smaller than that for δ = 0.005.

Figure 6(c) shows that as porous layer thickness $\hat{d}$ increases, the growth rate for the interface mode decreases; however, an increase in $\hat{d}$ changes the bimodal structure displayed by the dispersion curve of the porous mode to a unimodal structure and this is accompanied by a shift of the window of unstable wave numbers to long wavelength regimes [Fig. 6(d)]. The growth rate of the interface mode is not significantly affected by an increase in the anisotropy parameter ξ [Fig. 6(e)]. An increase in ξ preserves the two-humped shape of the dispersion curve in the moderate wave numbers [Fig. 6(f)]; there is stabilization in the low wave number regime with a further increase in ξ.

The investigation by Yiantsios and Higgins[3] predicts that two-layer viscosity-stratified flow of immiscible fluids in a channel is stable to long waves, when a thicker (thinner) layer hosts the more (less) viscous fluid. What happens to the stability characteristics when the bottom rigid wall in such a channel flow is replaced by a porous wall is of interest.

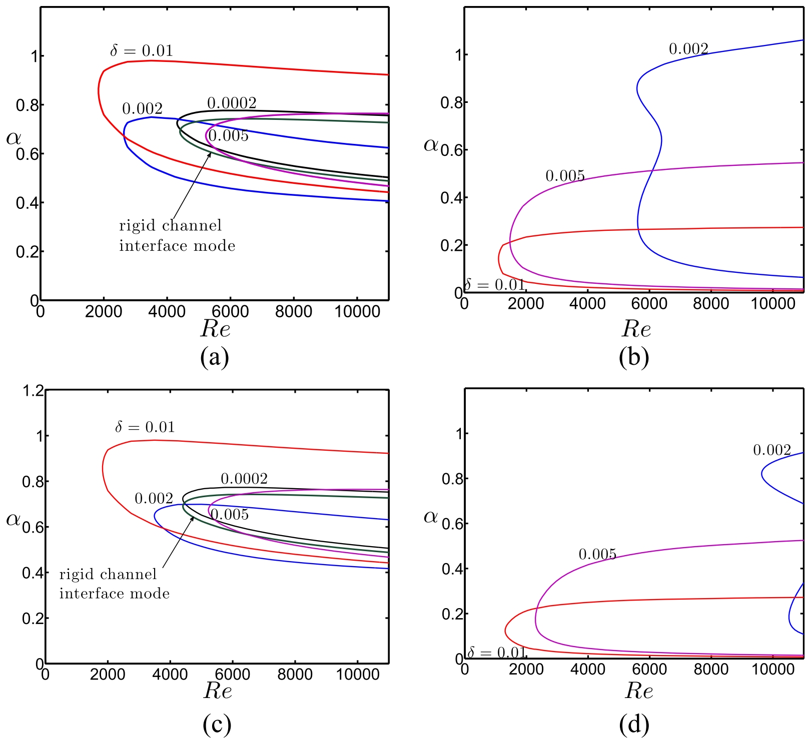

FIG. 7. Neutral stability boundaries for different permeabilities (δ = 0.01, 0.005, 0.002, 0.0002), in the $\alpha - Re$ plane when a high viscous fluid (m = 1.5) is in a thicker (n = 2) lower layer adjacent to the porous bottom. The other parameters are α_{BJ} = 0.1, ϕ = 0.3, r = 1, S = 0.1, $\hat{d}$ = 10, and A = 0, (a) ξ = 1, interface mode, (b) ξ = 1, porous mode, (c) ξ = 3 interface mode, and (d) ξ = 3, porous mode. The neutral stability curve for two-layer flow in a rigid channel is marked in the figure.

Figures 7(a)–7(d) present the neutral boundaries, when a high viscous fluid (m = 1.5) occupies a thicker lower layer (n = 2) adjacent to the porous channel wall. The parameters are fixed at α_{BJ} = 0.1, ϕ = 0.3, r = 1, S = 0.1, and $\hat{d}$ = 10. At $\hat{d}$ = 10 and n = 2, the porous layer is thicker than the adjacent lower layer. It is clear that the flow system is stable for all wave numbers in a window of low Reynolds numbers when the porous bottom is homogeneous and isotropic [Figs. 7(a) and 7(b)] and anisotropic [Figs. 7(c) and 7(d)]. When the porous channel wall is homogeneous (A = 0) and isotropic (ξ = 1), the flow perturbations permeate through the thicker porous layer; as a result, the porous mode destabilizes a bandwidth of low wave numbers at a higher permeability (δ = 0.01) beyond a critical value of Reynolds number, say, Re_p [the critical Reynolds number for the porous mode, Fig. 7(b)] and dominates the interface mode existing at moderate to O(1) wave number window beyond Re_i [the critical Reynolds number for the interface mode, Fig. 7(a)]. The reason for the dominance of porous mode at this large value of permeability can be understood as follows; the shear stress at the porous-liquid interface is weakened at this moderately large value of permeability (δ = 0.01); furthermore, there is a weakening of the resistance offered by the viscous force that arises due to the porous medium's solid phase. As a result, the fluid permeates easily through the porous medium. This causes reduction in the intensity of the instability induced by the interface and consequently the unstable porous mode dominates. The above trend is also observed for δ = 0.005; for this permeability, the bandwidth of unstable wave numbers decreases (increases) for the interface (porous) mode. With a further decrease in permeability (δ = 0.002), the interface mode dominates the coexisting porous mode and fluid layer mode occurring due to the confinement of flow perturbations in the fluid layer. The neutral boundary has a bi-modal shape at this value of δ [Fig. 7(b)]. These two modes coalesce with each other and destabilize higher Reynolds numbers for a wide range of wave numbers. The critical Reynolds number for the interface mode (Re_i) displays a non-monotonic trend as the permeability parameter is increased, for a system with a homogeneous and isotropic/anisotropic bottom wall [Figs. 7(a) and 7(c)]. Furthermore, in the parameter regimes where the interface mode is dominant, a configuration with a homogeneous and isotropic/anisotropic bottom wall can either destabilize or stabilize the corresponding system with a rigid bottom wall [as is evident from the neutral boundary for a rigid wall, Figs. 7(a) and 7(c)]; this neutral boundary has been obtained using the code developed to generate the results for the NSW case in Chattopadhyay and Usha.[25] The striking observation is that the two-layer flow in a rigid channel which is stable to long waves when a high viscous fluid occupies a thicker layer can be made unstable in the low wave number regimes by the presence of homogeneous and isotropic/anisotropic porous bottom wall at higher permeabilities. The existence of an unstable dominant porous mode in this region is responsible for destabilization of the long wave regime. As permeability decreases to δ = 0.0002, the porous mode disappears and there exists only the dominant unstable interface mode for the parameter values considered here. Note that

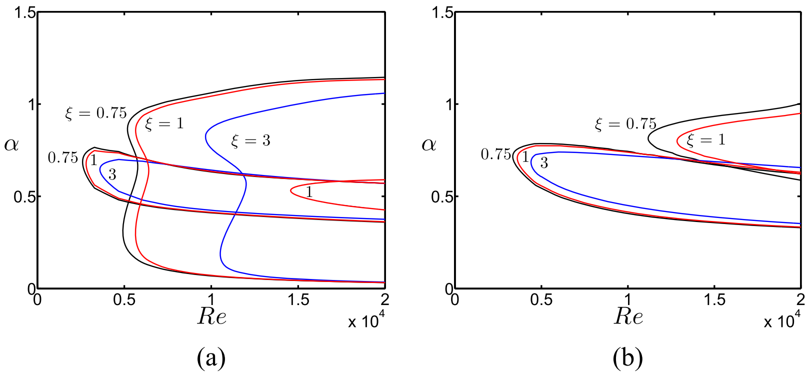

FIG. 8. Neutral stability boundaries for different values of the anisotropy parameter (ξ = 0.75, 1, 3), in the $\alpha - Re$ plane when a high viscous fluid (m = 1.5) is in a thicker (n = 2) lower layer adjacent to the porous medium. The other parameters are α_{BJ} = 0.1, ϕ = 0.3, r = 1, S = 0.1, δ = 0.002, and A = 0, (a) $\hat{d}$ = 10 and (b) $\hat{d}$ = 5.

decreasing the permeability enhances the viscous drag and this does not favour viscous diffusion of the momentum across the layer resulting in stabilization of the mode. The porous layer velocity is weaker than that in the liquid region, as permeability decreases.

Figures 7(c) and 7(d) reveal that anisotropic effects (ξ = 3, A = 0) stabilize the porous mode and the interface mode. This is because an increase in ξ corresponds to a decrease in permeability in the vertical direction, and this provides sufficient flow resistance, thus enabling stabilization. The stabilizing effect is more prominent for the porous mode at smaller permeability [δ = 0.002, Fig. 7(d)].

At this $\hat{d}$(= 10), enhancing the anisotropic (ξ) effects stabilizes the dominant interface mode [Figs. 7(a), 7(c), and 8(a)] which coexists with the coalescence of the porous and the fluid layer modes, displaying a bi-modal shape in the neutral stability boundary which is also stabilized. As ξ increases to ξ = 3 from ξ = 0.75, a local maximum occurs both at the lobe in the lower branch and at the lobe in the upper branch of the neutral stability boundary but the global maximum is at the upper branch of this neutral stability boundary. It is worth investigating that the changes arise due to a decrease in porous layer thickness [$\hat{d}$ = 5, Fig. 8(b)]. This results in an increase in critical Reynolds number (Re_i) when δ = 0.002, ξ = 1 keeping the other parameters the same as in Fig. 7(a). The long waves are stabilized for all Reynolds numbers. The porous mode disappears and the fluid mode destabilizes higher Reynolds numbers in a window of moderate to O(1) wave numbers. At this depth ratio ($\hat{d}$ = 5), an increase in the permeability in the mean flow direction (ξ increases) stabilizes the interface mode. Thus, incorporating anisotropy effects is found to stabilize both the porous and interface modes. This is because an increase in ξ corresponds to a decrease in permeability in the y-direction which provides sufficient flow resistance enabling stabilization.

Forced by the curiosity to see what happens to the stability of the porous mode if $\hat{d}$ is increased above or decreased below $\hat{d}$ = 10, the computations are performed and Fig. 9 presents the details for the system with homogeneous (A = 0) and isotropic (ξ = 1) porous bottom. It is interesting to note that while for $\hat{d}$ > 10, the low to moderate wave number regimes are destabilized for Reynolds numbers ranging from low to high values, only the short wave modes are destabilized at higher Reynolds numbers when $\hat{d}$ is decreased below 10. Both increase and decrease in $\hat{d}$ cause the bi-modal shaped neutral boundary to approach a uni-modal shape in different wave number regimes. As $\hat{d}$ decreases, the instability shifts from a low wave number mode in which the onset of instability occurs, to a high wave number mode. The same scenario is observed for variations in permeability, anisotropy, and inhomogeneity of the porous medium (figure not shown). The above results show that variations in $\hat{d}$ which corresponds to changes in porous layer thickness have a significant effect on the stability characteristics of the system considered. An increase in the thickness of the porous layer enhances this instability of the porous mode near long wave number region, whereas it stabilizes the disturbances due to fluid layer mode near short wave regime.

In order to understand the influence of permeability (δ) and anisotropy (ξ) of the porous bottom on the onset of instability (dominant unstable mode), the critical Reynolds number

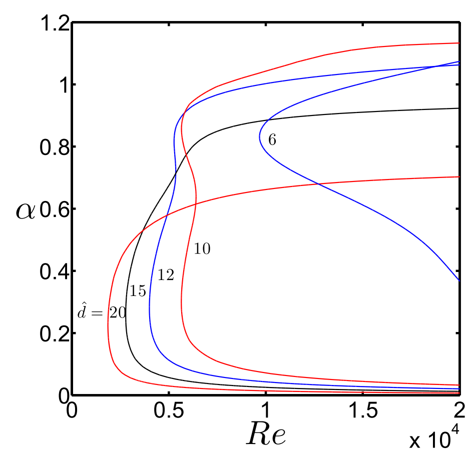

FIG. 9. The neutral stability boundaries for the porous mode, as the thickness ($\hat{d}$) of the homogeneous and isotropic porous layer increases when the other parameters are m = 1.5, n = 2, α_{BJ} = 0.1, ϕ = 0.3, r = 1, S = 0.1, and δ = 0.002.

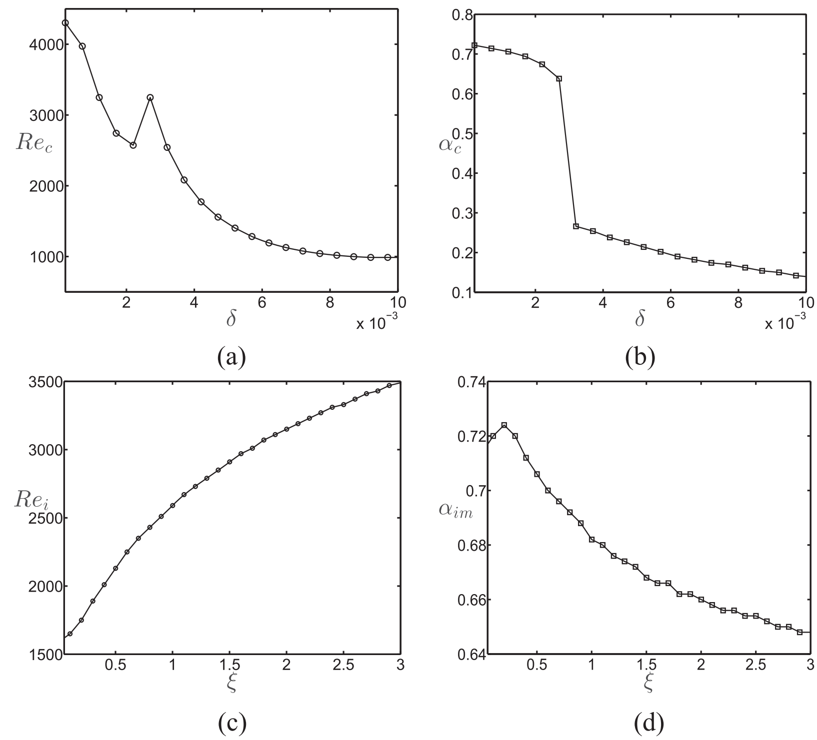

FIG. 10. Critical Reynolds number (Re_c) and the critical wave number (α_c) for the dominant unstable mode [(a) and (b)] influence of permeability δ of a homogeneous (A = 0) and isotropic (ξ = 1) porous bottom. [(c) and (d)] Influence of the anisotropy parameter (ξ) on the critical Reynolds number (Re_i) and critical wave number (α_{im}) when δ = 0.002. The porous bottom is homogeneous (A = 0). The other parameters are m = 1.5, n = 2, α_{BJ} = 0.1, ϕ = 0.3, r = 1, S = 0.1, and $\hat{d}$ = 10.

(Re_c), and the critical wave number (α_c) as a function of permeability [δ, Figs. 10(a) and 10(b)] and anisotropy parameter [ξ, Figs. 10(c) and 10(d)] are obtained and are presented in Figs. 10(a)–10(d). At small values of permeabilities, the critical wave number (α_c) decreases and is in a window of moderate wave numbers [Fig. 10(b)]. The critical Reynolds numbers decrease in this δ-window [Fig. 10(a)]. A close look at Figs. 7(a), 10(a), and 10(b) confirms that, in this δ-window, the dominant unstable mode is the interface mode for a system that hosts a high viscous fluid in a thicker lower layer adjacent to an isotropic (ξ = 1) and homogeneous (A = 0) porous bottom with depth ratio $\hat{d}$ = 10. The other parameters are α_{BJ} = 0.1, ϕ = 0.3, r = 1, and S = 0.1 in Fig. 10.

Taking a typical value of δ in this δ-window, namely, δ = 0.002, the critical Reynolds number (Re_i) and the critical wave number (α_{im}) for the interface mode are obtained. The decreasing trend of α_{im} [Fig. 10(d)] and the increasing trend of Re_i [Fig. 10(c)], as the anisotropy parameter ξ increases, indicate that the flow system with isotropic and homogeneous porous bottom can be stabilized by enhancing (decreasing) the permeability of the homogeneous porous bottom along the mean flow direction (transverse direction), keeping the other parameters the same as in Figs. 10(a) and 10(b). As δ increases further, the critical wave number α_c decreases further and is now in a window of small wave numbers [Fig. 10(b)]. The critical Reynolds number (Re_c) decreases in this δ-window [Fig. 10(a)], thereby destabilizing the system at low Reynolds numbers, indicating that the dominant unstable mode in this δ-window is the porous mode [as is evident from the results in Fig. 7(b)]. It is worth mentioning here that Tilton and Cortelezzi[20] have reported a similar trend for a critical Reynolds number and a critical wave number for single fluid Poiseuille flows in a porous channel. Increasing the permeability of the isotropic and homogeneous porous bottom with $\hat{d}$ = 10 results in switching of the dominance of the unstable mode for the flow system and the parameter values considered.

Figure 11(a) presents the critical Reynolds number for the dominant mode as a function of $\hat{d}$ for a typical value of permeability (δ = 0.002), when the porous bottom is homogeneous and isotropic. The interface mode is dominant till $\hat{d} \approx 13$ and beyond this $\hat{d}$, the porous mode is dominant. The critical Reynolds number for the dominant interface mode (Re_i) exhibits a non-monotonic behaviour in this $\hat{d}$-window, whereas the critical Reynolds number for the dominant porous mode (Re_p) decreases with an increase in $\hat{d}$ showing that it destabilizes the long waves at low Reynolds numbers. The critical wave number α_c as a function of $\hat{d}$ presented in Fig. 11(b) indicates that α_c decreases for both interface and porous modes, as thickness of the porous layer increases.

When a less viscous, thinner fluid layer (m = 0.8, n = 0.5; Fig. 12) is adjacent to the anisotropic porous layer (ξ = 0.75), with α_{BJ} = 0.1, ϕ = 0.3, δ = 0.002, then in the absence of inhomogeneity (A = 0), the porous, interface, and the fluid layer modes coalesce and a large unstable region covering a

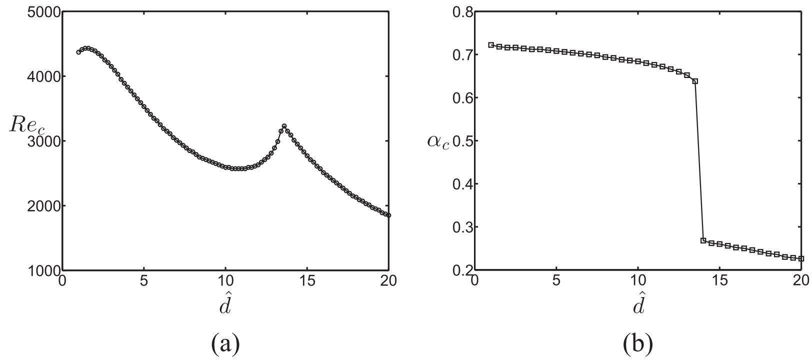

FIG. 11. Critical Reynolds number [Re_c; (a)] and the critical wave number [α_c; (b)] for the dominant unstable mode as a function of porous layer thickness $\hat{d}$, with the other parameters as m = 1.5, n = 2, α_{BJ} = 0.1, ϕ = 0.3, r = 1, S = 0.1, A = 0, δ = 0.002, and ξ = 1.

wide range of wave numbers and Reynolds numbers is seen, indicating that this configuration is more unstable than the one with high viscous fluid in a thicker layer adjacent to the porous layer at depth ratio $\hat{d}$ = 10. In contrast to the case, where m = 0.8, n = 0.5, there exists two unstable modes–the interface mode destabilizing a bandwidth of moderate wave numbers beyond Re_i and the coalescence of porous and fluid layer modes displaying bi-modal shape of neutral boundary destabilizing a large window covering low to O(1) wave numbers at moderate to large Reynolds numbers when m = 1.5, n = 2. At very large Re, we see a third mode, possibly, the shear mode/fluid layer mode making its appearance at moderate/O(1) wave numbers for m = 1.5, n = 2/m = 0.8, and n = 0.5, respectively.

At this stage, one is curious to understand the influence of relative volumetric flow rate in the two fluid layers with a high viscous fluid in the lower layer overlying a homogeneous, anisotropic porous bottom and Fig. 13 presents the details when $\alpha_{\rm BJ}$ = 0.1, ϕ = 0.3, r = 1, S = 0.1, δ = 0.002, and ξ = 0.75. The depth ratio is fixed at $\hat{d}$ = 10 with viscosity-stratification m = 1.5. The neutral stability boundary displays a bi-modal shape at n = 1.5, and a local maximum occurs at the lower branch as well as at the upper branch; the global maximum for the dominant mode of instability occurs in the lobe in the lower branch near the long-wave region (critical $Re \approx 4500$ and critical wave number $\alpha \approx 0.34$). As the depth of the lower layer increases (n = 2), the lobe at the upper branch is pushed towards the lower branch and the dominant mode of instability appears at the lobe in the lower branch (critical Reynolds number ≈ 4850 and critical wave number ≈ 0.3). The bi-modal neutral boundary encloses a bandwidth of unstable wave numbers at moderate to large Reynolds numbers. With a further increase in thickness of the lower layer, bi-modal shape still persists, but the lobe displaying local maximum at the upper branch in the short wave region is further pushed towards the lower branch close to the long-wave region and the dominant mode of instability appears in the short wave region, displaying the global maximum. At this depth ratio $\hat{d}$ = 10, the porous layer thickness is larger than that of the layer adjacent to it (for n = 1.5, 2, and 3). As the thickness of the lower layer increases with an increase in n, more disturbances penetrate into the lower layer dragging the upper branch towards smaller wave numbers. This results in pushing the unstable region near the upper branch to smaller Reynolds numbers and that near the lower branch to higher Reynolds numbers. At this value of n (n = 3), a new mode appears and destabilizes moderate to short waves at small to large Reynolds numbers.

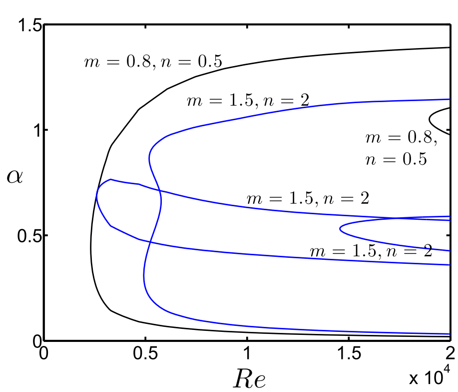

FIG. 12. Neutral stability boundaries for different viscosity ratios (m) and thickness ratios (n). The other parameters are α_{BJ} = 0.1, ϕ = 0.3, r = 1, S = 0.1, δ = 0.002, A = 0, ξ = 0.75, and $\hat{d}$ = 10.

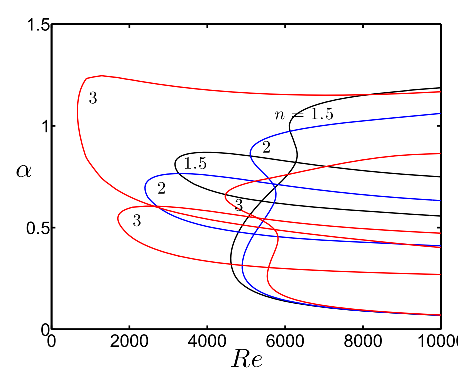

FIG. 13. Neutral stability boundaries in the $\alpha - Re$ plane for different relative volumetric flow rates as thickness ratio varies (n = 1.5, 2, 3), when a high viscous fluid (m = 1.5) is in the lower layer adjacent to the porous medium. The other parameters are α_{BJ} = 0.1, ϕ = 0.3, r = 1, S = 0.1, δ = 0.002, A = 0, ξ = 0.75, and $\hat{d}$ = 10.

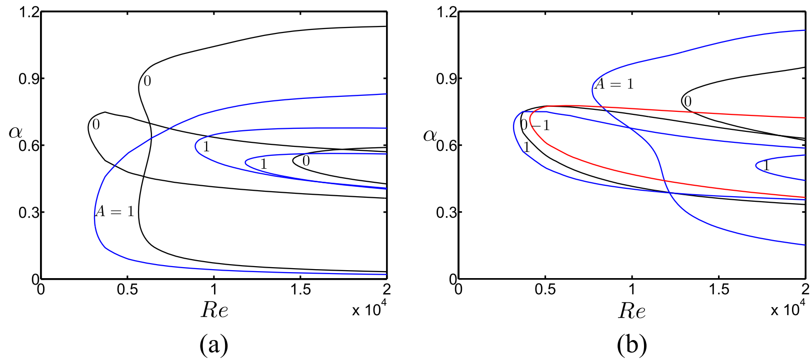

FIG. 14. Neutral stability boundaries in the $\alpha - Re$ plane for different inhomogeneities (A = 0, 1, −1) in the porous medium when a high viscous fluid (m = 1.5) is in a thicker (n = 2) lower layer adjacent to the porous medium. The other parameters are α_{BJ} = 0.1, ϕ = 0.3, r = 1, S = 0.1, δ = 0.002, and ξ = 1, (a) $\hat{d}$ = 10 and (b) $\hat{d}$ = 5.

At each n considered, an interface mode coexists destabilizing a window of moderate wave numbers beyond a critical Re_i and the critical Reynolds number for the interface mode decreases with increase in n. It is interesting to note that an increase in relative volumetric flow rate (n) results in switching the dominant mode from the interface mode to a new mode.

B. Two-layer flow in a channel with inhomogeneous and anisotropic porous bottom and rigid top

While for a system with a homogeneous, isotropic porous layer (ξ = 1 and A = 0), the interface mode is the dominant one and a bi-modal shaped neutral boundary encloses a large unstable region created due to the coalescence of porous and fluid layer modes, inclusion of inhomogeneity by increasing the permeability in the x and y-directions (A = 1) shifts the dominance to porous mode [Fig. 14(a)], when a high viscous fluid is in a thicker lower layer adjacent to the porous medium with $\hat{d}$ = 10. The parameters are fixed as α_{BJ} = 0.1, ϕ = 0.3, r = 1, S = 0.1, and δ = 0.002. This scenario is also accompanied by a change in the bandwidth of unstable wave numbers. The long waves are stabilized for small Reynolds numbers. The lobe at the upper branch almost disappears and the neutral stability boundary tends to have a uni-modal shape with its lobe near lower branch, being pushed to low Reynolds numbers, displaying a reduction in critical Reynolds number; this can be understood as due to lower flow resistance in the porous medium at this higher value of A(=1). The interface mode is stabilized at this value of A(=1) as is evident by the increase in critical Reynolds number as compared to that for A = 0.

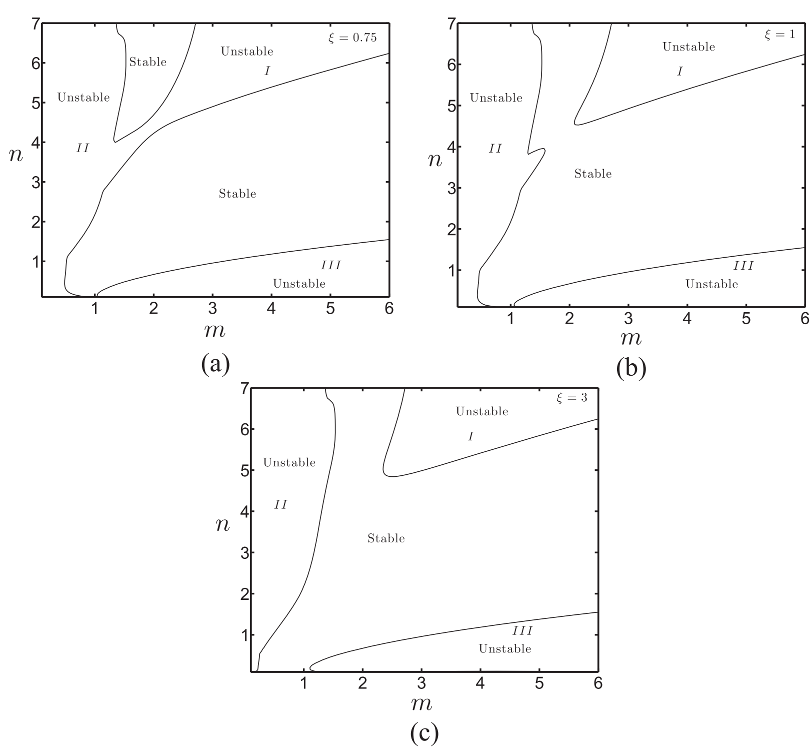

FIG. 15. Phase diagrams showing the stable and unstable regions at Re = 1500 and α = 0.5 in the m–n plane. The other parameters are α_{BJ} = 0.1, ϕ = 0.3, r = 1, S = 0.15, δ = 0.002, A = 0, and $\hat{d}$ = 10.

On the other hand, a decrease in the permeabilities in the x and y-directions (A = −1) results in stabilization of the flow system when $\hat{d}$ = 10 for a whole range of wave numbers and Reynolds numbers considered {neutral boundary does not appear in the regime of parameters considered in [Fig. 14(a)]}. This can be associated with the increased flow resistance in the porous medium at this value of A(=−1).

In the presence of inhomogeneity (A = 1), a reduction in depth ratio $\hat{d}$ (from $\hat{d}$ = 10 to $\hat{d}$ = 5) pushes the window of unstable wave numbers (the long-wave regime to moderate wave numbers) to a window from moderate to O(1) wave numbers. At this $\hat{d}$ ($\hat{d}$ = 5), there is no switching of the dominance of the unstable mode. The interface mode is the dominant unstable mode for $\hat{d}$ = 5, for all the values of A considered; but it is stabilized by an increase in permeability in the porous medium (A = 1); however, it is destabilized by decreasing the permeability along and transverse to the mean flow direction (A = −1).

When anisotropy effects are incorporated in a configuration with inhomogeneous porous bottom, the flow system is further destabilized for a decrease in ξ, which arises due to a decrease in permeability along the mean flow direction or an increase in permeability along the transverse direction. Note that an increase in ξ increases the critical Reynolds number and this is analogous to the scenario for a system with homogeneous anisotropic porous medium (figure not shown).

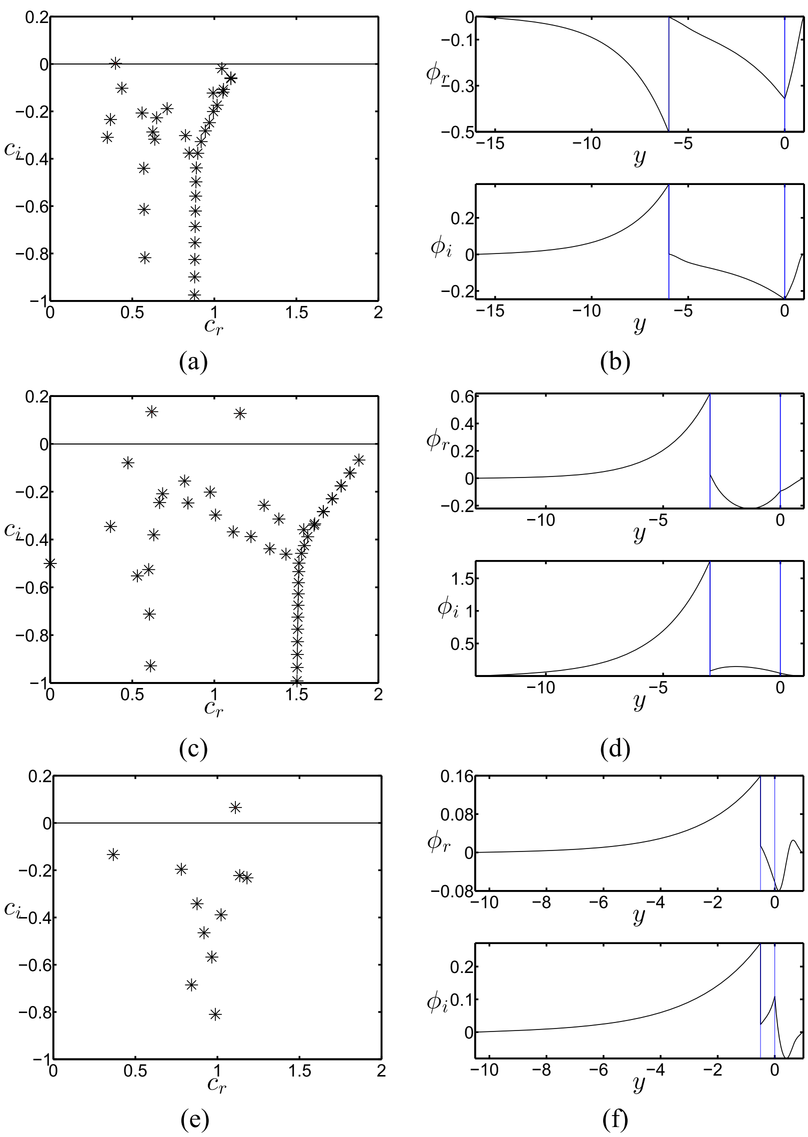

FIG. 16. The spectra and eigenfunctions in the unstable regions I–III in Fig. 15(a) with all parameter values same as Fig. 15(b), (a) spectrum at m = 4, n = 6, (b) eigenfunction at m = 4, n = 6, (c) spectrum at m = 0.5, n = 3, (d) eigenfunction at m = 0.5, n = 3, (e) spectrum at m = 3, n = 0.5, and (f) eigenfunction at m = 3, n = 0.5.

Figure 15 displays the boundaries separating the unstable and stable regions in the m–n plane at Re = 1500, α = 0.5, and $\hat{d}$ = 10 for a configuration with a porous bottom (homogeneous, A = 0) for three different values of anisotropy parameter ξ. The stable regions are well separated for ξ = 0.75 [Fig. 15(a)]. An increase in ξ results in merging of the stable regions and separation of unstable regions [ξ = 1, Fig. 15(b); ξ = 3, Fig. 15(c)]. The spectra [Figs. 16(a), 16(c), and 16(e)] and the corresponding profiles of the real (ϕ_r) and imaginary (ϕ_i) parts of the streamfunction disturbances are presented [Figs. 16(b), 16(d), and 16(f)], at typical points in the regions I (m = 4, n = 6), II (m = 0.5, n = 3), and III (m = 3, n = 0.5) marked in Fig. 15(a). This corresponds to examining the influence of relative magnitude of volumetric flow rate in the two fluid layers of different viscosities overlying the porous medium on the corresponding eigenfunctions (changes in thickness ratio, n). From the spectral figures on the left panels in Fig. 16, we see that a reduction in viscosity-stratification and thickness of the lower layer adjacent to the porous layer shifts the dominant unstable mode [Figs. 16(a) and 16(e)] from region I to region III and increases the wave speed c_r from $c_r < 1$ to $c_r > 1$. From the structure of the perturbation stream function at α = 0.5, we infer that the real parts of the stream function disturbance cover the whole region of the porous medium, they are localized near the liquid-liquid interface for the two-liquid layers. The amplitude of the perturbation streamfunction in the porous layer vanishes at the rigid support of the porous bottom and decreases monotonically within the porous layer. The amplitude of perturbation streamfunction in layer 2 (layer 1) vanishes at the liquid-porous interface (at the upper wall) and decreases monotonically till the liquid-liquid interface [Fig. 16(b)]. When the flow configuration holds a less viscous fluid (m = 0.5) in a thicker lower layer adjacent to the porous bottom, the above scenario is displayed but the amplitude monotonically increases within the porous layer, it decreases from its zero value at the liquid-porous interface to its value −0.2 at the center of the liquid layer 2 and beyond this it increases monotonically [Fig. 16(d)]. In this case, the co-existence of two unstable modes with one having $c_r < 1$ and the other with $c_r > 1$ is observed [Fig. 16(c)]. Furthermore, the critical motions of the streamfunction disturbances cover the porous layer as well as the whole of the two-fluid domains [Fig. 16(d)]. The corresponding values of ϕ_r are higher as compared to the other values of viscosity-stratification m and thickness ratio n considered in Figs. 16(b) and 16(f). For the three types of flow configurations considered, the dominant unstable mode induces disturbances and these propagate deep within the porous layer. This may be attributed to exchange of flux between the two-fluid layers and the porous layer.

V. CONCLUSION

We have analysed the linear temporal stability of a two-layer plane Poiseuille flow in a channel consisting of viscosity and/or density stratified, incompressible Newtonian fluids overlying an anisotropic and inhomogeneous porous bottom saturated by the fluid in the lower layer adjacent to it. The upper layer is bounded by a rigid wall. The dynamics in the porous layer is governed by the Darcy model with appropriate boundary conditions at the liquid-porous interface proposed by Beavers and Joseph,[58] which accounts for the discontinuity in the velocity between the fluid and the porous layers. The resulting Orr-Sommerfeld coupled eigenvalue problem is then numerically solved using a spectral collocation method and the significant characteristics of the stability of the stationary flow are examined. The features of instability are influenced (i) by the presence of the porous bottom, which alters the base flow velocity profiles as the parameters (δ, A, $\hat{d}$) characterizing the porous bottom are varied, (ii) by the nonzero velocity perturbations at the liquid porous interface, and (iii) by the perturbation at the liquid-liquid interface arising due to stratification in viscosity. As a result, the neutral boundaries are multi-branched in this system. A detailed parametric study revealed the co-existence of different types of modes: porous mode–manifests as a minimum in the neutral stability curve in the longwave regime, interface mode (triggered by the stratification of viscosity[97] across the liquid-liquid interface), fluid layer mode (existing in moderate wave numbers or O(1) wave numbers), and the shear mode and the coalescence of modes in different bandwidths of wave numbers and low to high Reynolds numbers. In the present study, we have focused on the features of instability (due to two-dimensional disturbances) of porous and interface modes and plan to discuss the details about other modes of instability in our future investigation.

Associated with changes in depth ratio $\hat{d}$, there is switching of the dominance of unstable mode (interface mode to porous mode as $\hat{d}$ increases; Fig. 11), for fixed permeability δ. While the critical Reynolds numbers (Re_p) for the dominant porous mode decrease with an increase in depth ratio, Re_i displays a nonmonotonic behaviour with respect to the depth ratio $\hat{d}$.

An increase in permeability of a homogeneous, isotropic/anisotropic porous layer results in a decrease in critical Reynolds number for the porous mode for a configuration with m = 1.5 in a thicker lower layer. This suggests that at permeabilities higher or equal to those considered in the present study, transition might be initiated by the mode that exists due to the presence of the porous mode. A dedicated and thorough non-linear analysis might shed more light on the above remark as it is known that there is a considerable reduction in the critical parameter values for the onset of instability predicted by the non-linear stability analysis as compared to those by linear temporal stability analysis and this also forms a part of our future study.

An increase in ξ corresponds to either a relative increase in permeability (K_x) in the x-direction or a relative decrease in permeability in the y-direction (K_y). A relative increase in permeability in the mean flow direction offers less resistance to flow disturbance at the fluid-porous layer interface and thus stabilizes the interface mode.

The two-layer flow in a rigid channel which is stable to longwaves when a highly viscous fluid occupies a thicker lower layer can become unstable at higher permeabilities (porous mode) to longwaves in a channel with a homogeneous and isotropic/anisotropic porous bottom and a rigid top. Due to sufficient flow resistance provided by a decrease in permeability in the vertical direction which occurs due to an increase in ξ, the porous and the interface modes are stabilized (Fig. 7). The critical Reynolds number, Re_i, and critical wave number, α_{im}, for the interface mode exhibit a nonmonotonic behaviour with respect to δ. However, Re_i increases with an increase in anisotropy parameter ξ indicating the stabilizing role of ξ in the interface mode for a flow system hosting a highly viscous, isodense fluid ($m = 1.5$, $r = 1$) in the thicker lower layer adjacent to a homogeneous porous bottom [Figs. 10(c) and 10(d)].

A decrease in viscosity-stratification makes the configuration hosting a less viscous fluid in a thinner lower layer near the porous bottom (homogeneous, anisotropic) to be more unstable than the one hosting a highly viscous fluid in a thicker lower layer.

An increase in thickness ratio n results in switching of the dominant mode from interface to fluid layer mode. An exponentially decreasing inhomogeneity in the permeability of the porous medium in the cross-stream direction is found to have effect on the interface modes. Longwaves are stabilized for all Reynolds numbers. An increase in A results in switching of dominant unstable mode (interface mode at A = 0 to porous mode at A = 1) for a thicker porous layer [Fig. 14(a)] resulting in destabilization of longwaves. The depth ratio has a crucial role in the primary instability. The depth ratio ($\hat{d} = d/d_1$) signifies the relative importance of the porous layer thickness as compared to the thickness of the upper fluid layer. It is evident that an increase in depth ratio is responsible for low wave number instability at smaller Reynolds numbers (Fig. 9), by the porous layer mode. The porous layer thickness thus has a destabilizing effect on the porous layer mode but plays a stabilizing role for the fluid-layer mode. An important feature of the obtained results is the bimodal structure displayed in the neutral stability boundaries, indicating the existence of longwave minima.

Switching of dominance of modes which arises due to variations in anisotropy (ξ) of the porous medium is dependent on the permeability (δ) and the depth ratio ($\hat{d}$). It is evident from the results that it is possible to exercise more control on the stability characteristics of the system by incorporating variations in permeability due to inhomogeneity than mean permeability modulations that arise due to changes in permeability parameter δ.

Inhomogeneity (due to an increase in vertical variation in permeability) renders short wave modes to become more unstable by enlarging the region of instability. This is in contrast to the anisotropic modulations (an increase in ξ) causing stabilization by both increasing the critical Reynolds number and shrinking the unstable region. Thus, we observe that the directional and spatial variations in permeability have a strong influence on the stability characteristics, for different depth ratios and ratio of thickness of fluid layers. A reduction in anisotropy destabilizes the system, but this trend is reversed with an increase in anisotropy parameter. A variation in inhomogeneity which enhances the overall permeability of the porous medium destabilizes the flow system. The stability properties can be exploited effectively in accordance with the relevant applications and thus facilitates the fabrication of devices involving two-layer channel flows. It is possible to stabilize/destabilize flows which were otherwise unstable/stable in a rigid channel by designing the walls as porous/rough for appropriate ratio of viscosity and layer thickness.

REFERENCES

[1] H. H. Hu and D. D. Joseph, "Lubricated pipelining: Stability of core-annular flow. Part 2," J. Fluid Mech. **205**, 359 (1989).

[2] P. Davidson and R. Lindsay, "Stability of interfacial waves in aluminium reduction cells," J. Fluid Mech. **362**, 273 (1998).

[3] S. G. Yiantsios and B. G. Higgins, "Linear stability of plane Poiseuille flow of two superposed fluids," Phys. Fluids **31**, 3225 (1988).

[4] T. W. Kao and C. Park, "Experimental investigations of the stability of channel flows. Part 1. Flow of a single liquid in a rectangular channel," J. Fluid Mech. **43**, 145 (1970).

[5] B. Tilley, S. Davis, and S. Bankoff, "Nonlinear long-wave stability of superposed fluids in an inclined channel," J. Fluid Mech. **277**, 55 (1994).

[6] A. Kaffel and A. Riaz, "Eigenspectra and mode coalescence of temporal instability in two-phase channel flow," Phys. Fluids **27**, 042101 (2015).

[7] C. Nouar, N. Kabouya, J. Dusek, and M. Mamou, "Modal and non-modal linear stability of the plane Bingham–Poiseuille flow," J. Fluid Mech. **577**, 211 (2007).

[8] R. Govindarajan and K. C. Sahu, "Instabilities in viscosity-stratified flow," Annu. Rev. Fluid Mech. **46**, 331 (2014).

[9] L. Danaila, L. Voivenel, and E. Varea, "Self-similarity criteria in anisotropic flows with viscosity stratification," Phys. Fluids **29**, 020716 (2017).

[10] B. Saikia, A. Ramachandran, K. Sinha, and R. Govindarajan, "Effects of viscosity and conductivity stratification on the linear stability and transient growth within compressible Couette flow," Phys. Fluids **29**, 024105 (2017).

[11] R. E. Ewing and S. Weekes, "Numerical methods for contaminant transport in porous media," Comput. Math. **202**, 75 (1998).

[12] M. B. Allen, *Collocation Techniques for Modeling Compositional Flows in Oil Reservoirs* (Springer, New York, 1984).

[13] B. Myron III, G. A. Behie, and J. A. Trangenstein, *Multiphase Flow in Porous Media: Mechanics, Mathematics, and Numerics* (Springer Science & Business Media, New York, 2013).

[14] D. Blest, B. Duffy, S. McKee, and A. Zulkifle, "Curing simulation of thermoset composites," Composites, Part A **30**, 1289 (1999).

[15] D. Blest, S. McKee, A. Zulkifle, and P. Marshall, "Curing simulation by autoclave resin infusion," Compos. Sci. Technol. **59**, 2297 (1999).

[16] B. Chen *et al.*, "Two-dimensional modeling of microscale transport and biotransformation in porous media," Numer. Methods Partial Differ. Equations **10**, 65 (1994).

[17] B. J. Suchomel, B. M. Chen, and M. B. Allen, "Network model of flow, transport and biofilm effects in porous media," Transp. Porous Media **30**, 1 (1998).

[18] E. Miglio, A. Quarteroni, and F. Saleri, "Coupling of free surface and groundwater flows," Comput. Fluids **32**, 73 (2003).

[19] F. Boano, R. Revelli, and L. Ridolfi, "Bedform-induced hyporheic exchange with unsteady flows," Adv. Water Resour. **30**, 148 (2007).

[20]N. Tilton and L. Cortelezzi, "Linear stability analysis of pressure-driven flows in channels with porous walls," J. Fluid Mech. **604**, 411 (2008).
[21]N. Tilton and L. Cortelezzi, "The destabilizing effects of wall permeability in channel flows: A linear stability analysis," Phys. Fluids **18**, 051702 (2006).
[22]P. Deepu, S. Dawande, and S. Basu, "Instabilities in a fluid overlying an inclined anisotropic and inhomogeneous porous layer," J. Fluid Mech. **762**, R2 (2015).
[23]A. Samanta, "Role of slip on the linear stability of a liquid flow through a porous channel," Phys. Fluids **29**, 094103 (2017).
[24]A. A. P. Kumar, H. Goyal, T. Banerjee, and D. Bandyopadhyay, "Instability modes of a two-layer Newtonian plane Couette flow past a porous medium," Phys. Rev. E **87**, 063003 (2013).
[25]G. Chattopadhyay and R. Usha, "On the Yih–Marangoni instability of a two-phase plane Poiseuille flow in a hydrophobic channel," Chem. Eng. Sci. **145**, 214 (2016).
[26]A. Goharzadeh, A. Khalili, and B. B. Jørgensen, "Transition layer thickness at a fluid-porous interface," Phys. Fluids **17**, 057102 (2005).
[27]B. Berkowitz, "Characterizing flow and transport in fractured geological media: A review," Adv. Water Resour. **25**, 861 (2002).
[28]J. Majdalani, C. Zhou, and C. A. Dawson, "Two-dimensional viscous flow between slowly expanding or contracting walls with weak permeability," J. Biomech. **35**, 1399 (2002).
[29]H. N. Chang, J. S. Ha, J. K. Park, I. H. Kim, and H. D. Shin, "Velocity field of pulsatile flow in a porous tube," J. Biomech. **22**, 1257 (1989).
[30]P.-X. Jiang, L. Yu, J.-G. Sun, and J. Wang, "Experimental and numerical investigation of convection heat transfer in transpiration cooling," Appl. Therm. Eng. **24**, 1271 (2004).
[31]R. D. Joslin, "Aircraft laminar flow control," Annu. Rev. Fluid Mech. **30**, 1 (1998).
[32]F. Chen and C. Chen, "Onset of finger convection in a horizontal porous layer underlying a fluid layer," J. Heat Transfer **110**, 403 (1988).
[33]B. Myron III, *Collocation Techniques for Modeling Compositional Flows in Oil Reservoirs* (Springer Science & Business Media, New York, 2013).
[34]V. Nassehi, "Modelling of combined Navier–Stokes and Darcy flows in crossflow membrane filtration," Chem. Eng. Sci. **53**, 1253 (1998).
[35]H. Squire and S. Goldstein, *Modern Developments in Fluid Dynamics* (Oxford University Press, New York, 1938).
[36]S. Granick, Y. Zhu, and H. Lee, "Slippery questions about complex fluids flowing past solids," Nat. Mater. **2**, 221 (2003).
[37]P. Tabeling, "Slip phenomena at liquid-solid interfaces," C. R. Phys. **5**, 531 (2004).
[38]E. Lauga and C. Cossu, "A note on the stability of slip channel flows," Phys. Fluids **17**, 088106 (2005).
[39]O. I. Vinogradova, "Slippage of water over hydrophobic surfaces," Int. J. Miner. Process. **56**, 31 (1999).
[40]T. D. Blake, "Slip between a liquid and a solid: D.M. Tolstoi's (1952) theory reconsidered," Colloids Surf. **47**, 135 (1990).
[41]R. S. Voronov, D. V. Papavassiliou, and L. L. Lee, "Review of fluid slip over superhydrophobic surfaces and its dependence on the contact angle," Ind. Eng. Chem. Res. **47**, 2455 (2008).
[42]O. I. Vinogradova, "Drainage of a thin liquid film confined between hydrophobic surfaces," Langmuir **11**, 2213 (1995).
[43]E. Ruckenstein and P. Rajora, "On the no-slip boundary condition of hydrodynamics," J. Colloid Interface Sci. **96**, 488 (1983).
[44]D. C. Tretheway and C. D. Meinhart, "Apparent fluid slip at hydrophobic microchannel walls," Phys. Fluids **14**, L9 (2002).
[45]K. Watanabe and H. Udagawa, "Drag reduction of non-Newtonian fluids in a circular pipe with a highly water-repellent wall," AIChE J. **47**, 256 (2001).
[46]T. Min and J. Kim, "Effects of hydrophobic surface on stability and transition," Phys. Fluids **17**, 108106 (2005).
[47]A. A. Hill and B. Straughan, "Poiseuille flow in a fluid overlying a porous medium," J. Fluid Mech. **603**, 137 (2008).
[48]M.-H. Chang, F. Chen, and B. Straughan, "Instability of Poiseuille flow in a fluid overlying a porous layer," J. Fluid Mech. **564**, 287 (2006).
[49]D. A. Nield and A. Bejan, *Convection in Porous Media* (Springer, New York, 2006).
[50]A. A. Hill and B. Straughan, "Global stability for thermal convection in a fluid overlying a highly porous material," Proc. R. Soc. A **465**, 207–217 (2008).
[51]S. A. Orszag, "Accurate solution of the Orr–Sommerfeld stability equation," J. Fluid Mech. **50**, 689 (1971).
[52]J. Dongarra, B. Straughan, and D. Walker, "Chebyshev tau-QZ algorithm methods for calculating spectra of hydrodynamic stability problems," Appl. Numer. Math. **22**, 399 (1996).
[53]R. Liu, Q. S. Liu, and S. C. Zhao, "Instability of plane Poiseuille flow in a fluid-porous system," Phys. Fluids **20**, 104105 (2008).
[54]M. Badiey, A. H.-D. Cheng, and I. Jaya, "Deterministic and stochastic analyses of acoustic plane-wave reflection from inhomogeneous porous seafloor," J. Acoust. Soc. Am. **99**, 903 (1996).
[55]M. Malashetty and M. Swamy, "The onset of convection in a binary fluid saturated anisotropic porous layer," Int. J. Therm. Sci. **49**, 867 (2010).
[56]P. Deepu, P. Anand, and S. Basu, "Stability of Poiseuille flow in a fluid overlying an anisotropic and inhomogeneous porous layer," Phys. Rev. E **92**, 023009 (2015).
[57]F. Chen and L. H. Hsu, "Onset of thermal convection in an anisotropic and inhomogeneous porous layer underlying a fluid layer," J. Appl. Phys. **69**, 6289 (1991).
[58]G. S. Beavers and D. D. Joseph, "Boundary conditions at a naturally permeable wall," J. Fluid Mech. **30**, 197 (1967).
[59]E. M. Sparrow, G. Beavers, T. Chen, and J. Lloyd, "Breakdown of the laminar flow regime in permeable-walled ducts," J. Appl. Mech. **40**, 337 (1973).
[60]C. Deng and D. M. Martinez, "Linear stability of a Berman flow in a channel partially filled with a porous medium," Phys. Fluids **17**, 024102 (2005).
[61]G. S. Beavers, E. M. Sparrow, and R. A. Magnuson, "Experiments on coupled parallel flows in a channel and a bounding porous medium," J. Basic Eng. **92**, 843 (1970).
[62]N. Silin, J. Converti, D. Dalponte, and A. Clausse, "Flow instabilities between two parallel planes semi-obstructed by an easily penetrable porous medium," J. Fluid Mech. **689**, 417 (2011).
[63]H. Goyal, P. Ananth, D. Bandyopadhyay, R. Usha, and T. Banerjee, "Instabilities of a confined two-layer flow on a porous medium: An Orr–Sommerfeld analysis," Chem. Eng. Sci. **97**, 109 (2013).
[64]B. Straughan and D. Walker, "Anisotropic porous penetrative convection," Proc. R. Soc. London, Ser. A **452**, 97 (1996).
[65]J. A. Ochoa-Tapia and S. Whitaker, "Momentum transfer at the boundary between a porous medium and a homogeneous fluid—I. Theoretical development," Int. J. Heat Mass Transfer **38**, 2635 (1995).
[66]B. Goyeau, D. Lhuillier, D. Gobin, and M. Velarde, "Momentum transport at a fluid–porous interface," Int. J. Heat Mass Transfer **46**, 4071 (2003).
[67]M.-H. Chang, "Thermal convection in superposed fluid and porous layers subjected to a horizontal plane Couette flow," Phys. Fluids **17**, 064106 (2005).
[68]U. Thiele, B. Goyeau, and M. G. Velarde, "Stability analysis of thin film flow along a heated porous wall," Phys. Fluids **21**, 014103 (2009).
[69]R. Liu and Q. Liu, "Instabilities and transient behaviors of a liquid film flowing down a porous inclined plane," Phys. Fluids **22**, 074101 (2010).
[70]Anjalaiah, R. Usha, and S. Millet, "Thin film flow down a porous substrate in the presence of an insoluble surfactant: Stability analysis," Phys. Fluids **25**, 022101 (2013).
[71]A. Samanta, B. Goyeau, and C. Ruyer-Quil, "A falling film on a porous medium," J. Fluid Mech. **716**, 414 (2013).
[72]R. Usha and S. Naire, "A thin film on a porous substrate: A two-sided model, dynamics and stability," Chem. Eng. Sci. **89**, 72 (2013).

[73] D. Nield, "Onset of convection in a fluid layer overlying a layer of a porous medium," J. Fluid Mech. **81**, 513 (1977).
[74] D. A. Nield, "The boundary correction for the Rayleigh-Darcy problem: Limitations of the Brinkman equation," J. Fluid Mech. **128**, 37 (1983).
[75] D. Nield, "The limitations of the Brinkman-Forchheimer equation in modeling flow in a saturated porous medium and at an interface," Int. J. Heat Fluid Flow **12**, 269 (1991).
[76] D. Nield, "Modelling the effect of surface tension on the onset of natural convection in a saturated porous medium," Transp. Porous Media **31**, 365 (1998).
[77] M. Carr, "Penetrative convection in a superposed porous-medium–fluid layer via internal heating," J. Fluid Mech. **509**, 305 (2004).
[78] M. Carr and B. Straughan, "Penetrative convection in a fluid overlying a porous layer," Adv. Water Resour. **26**, 263 (2003).
[79] B. Straughan, "Effect of property variation and modelling on convection in a fluid overlying a porous layer," Int. J. Numer. Anal. Methods Geomech. **26**, 75 (2002).
[80] S. Hirata, B. Goyeau, D. Gobin, M. Carr, and R. M. Cotta, "Linear stability of natural convection in superposed fluid and porous layers: Influence of the interfacial modelling," Int. J. Heat Mass Transfer **50**, 1356 (2007).
[81] H. Brinkman, "A calculation of the viscous force exerted by a flowing fluid on a dense swarm of particles," Flow, Turbul. Combust. **1**, 27 (1949).
[82] G. Neale and W. Nader, "Practical significance of Brinkman's extension of Darcy's law: Coupled parallel flows within a channel and a bounding porous medium," Can. J. Chem. Eng. **52**, 475 (1974).
[83] T. Desaive, G. Lebon, and M. Hennenberg, "Coupled capillary and gravity-driven instability in a liquid film overlying a porous layer," Phys. Rev. E **64**, 066304 (2001).
[84] R. Larson and J. Higdon, "Microscopic flow near the surface of two-dimensional porous media. Part 1. Axial flow," J. Fluid Mech. **166**, 449 (1986).
[85] R. Larson and J. Higdon, "Microscopic flow near the surface of two-dimensional porous media. Part 2. Transverse flow," J. Fluid Mech. **178**, 119 (1987).
[86] M. Kaviany, *Principles of Heat Transfer in Porous Media* (Springer Science & Business Media, New York, 2012).
[87] M. G. Worster, "Instabilities of the liquid and mushy regions during solidification of alloys," J. Fluid Mech. **237**, 649 (1992).
[88] H. Emami-Meybodi, "Dispersion-driven instability of mixed convective flow in porous media," Phys. Fluids **29**, 094102 (2017).
[89] Y. Qin and P. Kaloni, "Creeping flow past a porous spherical shell," ZAMM-J. Appl. Math. Mech./Z. Angew. Math. Mech. **73**, 77 (1993).
[90] M. Discacciati, E. Miglio, and A. Quarteroni, "Mathematical and numerical models for coupling surface and groundwater flows," Appl. Numer. Math. **43**, 57 (2002).
[91] D. Das, V. Nassehi, and R. Wakeman, "A finite volume model for the hydrodynamics of combined free and porous flow in sub-surface regions," Adv. Environ. Res. **7**, 35 (2002).
[92] W. J. Layton, F. Schieweck, and I. Yotov, "Coupling fluid flow with porous media flow," SIAM J. Numer. Anal. **40**, 2195 (2002).
[93] J. A. Ochoa-Tapia and S. Whitaker, "Momentum transfer at the boundary between a porous medium and a homogeneous fluid—II. Comparison with experiment," Int. J. Heat Mass Transfer **38**, 2647 (1995).
[94] F. Chen, "Salt-finger instability in an anisotropic and inhomogeneous porous substrate underlying a fluid layer," J. Appl. Phys. **71**, 5222 (1992).
[95] T. Green and R. L. Freehill, "Marginal stability in inhomogeneous porous media," J. Appl. Phys. **40**, 1759 (1969).
[96] P. J. Schmid and D. S. Henningson, *Stability and Transition in Shear Flows* (Springer Science & Business Media, New York, 2012).
[97] C.-S. Yih, "Instability due to viscosity stratification," J. Fluid Mech. **27**, 337 (1967).